

Distance measurements to early-type galaxies by improving the fundamental plane

Christoph Saulder,¹* Ian Steer,² Owain Snaith,³ Changbom Park,¹

¹*Korea Institute for Advanced Study, 85 Hoegiro, Dongdaemun-gu, 02455 Seoul, Republic of Korea*

²*NASA/IPAC Extragalactic Database, Pasadena, California, USA*

³*GEPI, Observatoire de Paris, Université PSL, CNRS, 5 Place Jules Janssen, 92190 Meudon, France*

Accepted XXX. Received YYY; in original form ZZZ

ABSTRACT

Using SDSS DR15 to its full extent, we derived fundamental plane distances to over 317 000 early-type galaxies up to a redshift of 0.4. In addition to providing the largest sample of fundamental plane distances ever calculated, as well as a well calibrated group catalogue covering the entire SDSS spectroscopic footprint as far a redshift of 0.5, we present several improvements reaching beyond the traditional definition of the fundamental plane. In one approach, we adjusted the distances by removing systematic biases and selection effects in redshift-magnitude space, thereby greatly improving the quality of measurements. Alternatively, by expanding the traditional fundamental plane by additional terms, we managed to remove systematic biases caused by the selection of our SDSS spectroscopic galaxy sample as well as notably reducing its scatter. We discuss the advantages and caveats of these various methods and calibrations in detail. We found that improving the fundamental plane distance estimates beyond the established methods requires a delicate balancing act between various systematic biases and gains, but managed to reduce the uncertainty of our distance measurements by about a factor of two compared to the traditional fundamental plane.

Key words: galaxies: elliptical and lenticular, cD – galaxies: distances and redshifts – galaxies: fundamental parameters – galaxies: statistics –

1 INTRODUCTION

The increasing number of galaxies covered by large-scale spectroscopic surveys (Aguado et al. 2018; Dawson et al. 2013) provides an opportunity to revisit the fundamental plane of early-type galaxies and to explore new ideas on how to improve this scaling relation as a distance indicator. Furthermore, various other surveys and programmes have accumulated a huge amount of additional distance information, to which we can compare our data.

During the pioneering work on the scaling-relations of early-type galaxies, the Faber-Jackson relation (Faber & Jackson 1976; Schechter 1980; Tonry & Davis 1981) and the Kormendy relation (Kormendy 1977) were discovered. Nowadays, they are seen as projections of the fundamental plane, which was properly defined and discussed in Dressler et al. (1987) and Djorgovski & Davis (1987), after being first mentioned in Terlevich et al. (1981). Its functional form is often given in the following way:

$$\log_{10}(R_e) = a \cdot \log_{10}(\sigma_0) + b \cdot \mu_e + c. \quad (1)$$

The fundamental plane is an empirical relation between three global parameters of elliptical galaxies: the central velocity dispersion σ_0 , the physical effective radius R_e , and the mean surface brightness

μ_e within the effective radius, which is occasionally written as $\log_{10}(I_e) = -\mu_e/2.5$ in the literature¹. The coefficients a , b , and c of the fundamental plane are obtained by fitting the relation to some set of early-type galaxies, whose distances are (approximately) known due to another distance indicator. The central velocity dispersion and the mean surface brightness² are distance-independent quantities. Consequently, one can use the fundamental plane as a distance indicator (standard rod) by comparing the predicted effective radius with the observed one. After its discovery the fundamental plane quickly became a complementary tool to the Tully-Fisher relation (Tully & Fisher 1977), which uses late-type galaxies, for measuring extragalactic distances.

From a more theoretical point of view, the Virial equilibrium predicts correlations between the three parameters R_e , σ_0 , and μ_e . Assuming a constant luminosity-independent mass-to-light (M/L) ratio for all early-type galaxies, the virial equilibrium condition would predict the following values for the coefficients: $a = 2$ and $b = 0.4$. In the literature, one typically finds values for a ranging between 1 and 1.5 (depending on the fitting method) and for b around

¹ The corresponding fundamental plane coefficient $b' = -2.5b$ is then called b in the literature, which can lead to some confusion.

² Corrected for the Tolman-effect, which is a cosmological effect that dims surface brightness proportional to $(1+z)^4$.

*E-mail: csaulder@kias.re.kr

0.3 (Saulder et al. 2013). This discrepancy between the theoretical prediction and observations is called the tilt of the fundamental plane. The reasons for this tilt have been a matter of substantial debate, especially in the context of galaxy evolution (Ciotti et al. 1996; Busarello et al. 1997, 1998; Graham & Colless 1997; Trujillo et al. 2004; D’Onofrio et al. 2006; Cappellari et al. 2006; Magoulas et al. 2013) or environmental dependence (Lucey et al. 1991; Jorgensen et al. 1996; Pahre et al. 1998; de Carvalho & Djorgovski 1992; La Barbera et al. 2010b; Magoulas et al. 2013; Hou & Wang 2015; Joachimi et al. 2015; Samir et al. 2016; Kipper et al. 2016). The fundamental plane is still a topic of ongoing research (D’Onofrio et al. 2008; La Barbera et al. 2008; Gargiulo et al. 2009; Hyde & Bernardi 2009b; La Barbera et al. 2010a; Fraix-Burnet et al. 2010; Magoulas et al. 2012; Hyde & Bernardi 2009a; Cappellari et al. 2013) and there have been numerous discussions (Jørgensen et al. 1993; Jorgensen et al. 1996; Jørgensen et al. 2006; Pahre et al. 1998; Bolton et al. 2008; D’Onofrio et al. 2013, 2017) on how to understand this scaling relation. Recently, the focus has shifted towards studying the formation (Bezanson et al. 2013; van de Sande et al. 2014; Beifiori et al. 2015, 2017) and evolution (Zahid et al. 2015, 2016; Oldham et al. 2017) of the fundamental plane and how to reconcile observations with simulations (Taranu et al. 2015; Desmond & Wechsler 2017). Our understanding of early-type galaxies has significantly improved during the last decade. Thanks to the first integral field spectroscopic surveys (Bacon et al. 2001; Cappellari et al. 2011), it became clear that the majority of early-type galaxies exhibit significant rotation (Emsellem et al. 2011; Cappellari et al. 2007) and are not primarily pressure-supported systems. Furthermore, the importance of stellar populations (Springob et al. 2012) and the luminosity dependence of the mass-to-light ratio (Hyde & Bernardi 2009b; Cappellari et al. 2013; Schechter et al. 2014; Desmond & Wechsler 2017) of early-type galaxies became crucial in understanding the tilt and the scatter of the fundamental plane. Additionally, it was found by Padmanabhan et al. (2004) and Gallazzi et al. (2006) that the stellar-to-dynamical mass ratio is not constant across all populations of early-type galaxies and D’Onofrio et al. (2008) and Nigoche-Netro et al. (2009) showed that the fundamental plane depends on the range in velocity dispersion and luminosity. A constant stream of data coming in and being analysed from currently ongoing big integral field spectroscopic surveys (Bundy et al. 2015; Croom et al. 2012) drives the improvement of our knowledge about very complex interplay between the global parameters of early-type galaxies and their internal kinematics (Scott et al. 2015; van de Sande et al. 2017; Graham et al. 2018). Additionally, some modifications of gravity are discussed as alternatives (Jovanović et al. 2016; Chiu et al. 2017) to a luminosity dependence of the mass-to-light ratio. Furthermore, a connection between the stellar and dark matter halo has also been proposed (Schechter 2016) to explain the shape of the fundamental plane.

Since its discovery, the coefficients of the fundamental plane have been calibrated using various samples, ever increasing in size or quality. For example, some of the most notable works providing these coefficients are Djorgovski & Davis (1987); Dressler et al. (1987); Smith et al. (2001, 2004); Hudson et al. (1997); Gibbons et al. (2001); Lucey et al. (1991); Guzman et al. (1993); Jorgensen et al. (1996); Müller et al. (1998); D’Onofrio et al. (2008); La Barbera et al. (2008); Gargiulo et al. (2009); Hyde & Bernardi (2009b); La Barbera et al. (2010a); Pahre et al. (1998); Kelson et al. (2000); Colless et al. (2001); Bernardi et al. (2003); Magoulas et al. (2012); Campbell et al. (2014); Scodreggio et al. (1998); Fraix-Burnet et al. (2010); Saulder et al. (2013, 2015); Zahid et al. (2016). The actual values of the coefficients vary notably due to the different

fitting methods (Sheth & Bernardi 2012), but for the application as a distance indicator a direct fit (Bernardi et al. 2003; Sheth & Bernardi 2012) that minimizes scatter in the physical radius R_e is the optimal choice, because it directly translates into a scatter in distances. The fundamental plane can be used as an efficient tool to measure peculiar motions in the local universe (Campbell et al. 2014; Mutabazi et al. 2014).

The Sloan Digital Sky Survey (SDSS) has been continuously providing new data and made its DR15 (Aguado et al. 2018) recently available to the public. While not including new galaxies in our range of interest since the completion of BOSS (Dawson et al. 2013), it provides updated photometric and spectroscopic fits for all galaxies. The previously largest sample of fundamental plane distances published along with a limited group catalogue in Saulder et al. (2016) was effectively limited to the sample size of DR7 (Abazajian et al. 2009) by the use of GalaxyZoo-I (Lintott et al. 2008). By improving the selection criteria for early-type galaxies, one will be able to cover many galaxies for which fundamental plane distance have never been calculated. Furthermore, it provides an opportunity to improve the quality of the distance measurements using the fundamental plane by better considering the selection effects of SDSS. Different methods for calibrations can be tested, as well as how to best take into account known biases affecting the fundamental plane, such the impact of the mass-to-light ratio (Hyde & Bernardi 2009b; Cappellari et al. 2013; Schechter et al. 2014; Desmond & Wechsler 2017) and environmental effects (Joachimi et al. 2015). To investigate the latter, a state-of-the-art group catalogue that covers at least the same volume as the early-type galaxies used for the fundamental plane is required. This can also be used to further improve the distance estimates to rich clusters by using statistics.

Throughout this paper, we assumed a flat Λ -CDM cosmology with a relative dark energy density of $\Omega_\Lambda = 0.7$ and a relative matter density of $\Omega_M = 0.3$ as well as a present-day Hubble parameter of $H_0 = 70 \text{ km s}^{-1} \text{ Mpc}^{-1}$.

This paper is structured in the following way: in Section 2, we present a description of the various datasets used for this work, with additional details provided in Appendix A. Our methods are explained in Section 3. We present the main results of our work in Section 4 with a more detailed description of our catalogues provided in Appendix B. We discuss our methods and results in Section 5 and provide a brief summary and conclusions in Section 6. Alternative approaches that we tested are briefly discussed in Appendix C as well as transformations between SDSS and 2MRS colours that were required as a tool are provided in Appendix D.

2 DATA

Our primary source of data was SDSS DR15 (Aguado et al. 2018) from which we selected an essentially unconstrained (aside from the intrinsic selection criteria of SDSS) spectroscopic sample of galaxies up to a redshift of 0.51³ as well as a sample of early-type galaxies, defined by colour-cuts and likelihoods for luminosity profile fits. Additionally, we used the value-added catalogue by Graham et al. (2018), which is based on MaNGA data (Bundy et al. 2015), and the value-added catalogue by Simard et al. (2011), which provides additional parameters for SDSS galaxies. For the calibration of

³ This value was reduced to 0.5 after the redshifts had been moved to the CMB rest frame to avoid an anisotropic cut-off.

our group finder algorithm, we also required simulated data. To this end, we took the re-run of the Millennium simulation (Springel et al. 2005) presented by Guo et al. (2013), who updated it to the WMAP7 cosmology (Komatsu et al. 2011). Several additional datasets are used for comparison and testing of our derived distances.

The mostly unfiltered galaxy sample was used to run our group finder algorithm. The resulting group catalogue may also be used for applications beyond the scope of this paper. We selected galaxies in SDSS DR15 using the set of criteria listed in Appendix A. With these criteria we found 1 527 251 objects (see Figure 1) in SDSS, for which we obtained their positions and basic photometric parameters (see Appendix A for a detailed list).

Our sample of early-type galaxies is a subsample of the previous galaxy sample, hence all the above criteria were applied. Additionally, we required these galaxies to fulfil the set of criteria presented in Appendix A2. With these selection criteria, we found 334 388 objects (see Figure 1) in the SDSS database. Additional constraints (finer cuts) were applied later in the calibration process to remove outliers and possible misclassifications. For the selected objects, we obtained their coordinates, basic spectroscopic and photometric parameters, and their stellar masses according to spectro-photometric Wisconsin method (Chen et al. 2012) using Maraston stellar mass models (Maraston & Strömbäck 2011). A detailed list of the obtained parameters is provided in Appendix A2. This sample of early-type galaxies formed the basis for our fundamental plane calibrations.

Graham et al. (2018) published a catalogue providing additional kinematic parameters for 2 774 galaxies, which were observed using integral-field spectroscopy as part of the MaNGA programme (Bundy et al. 2015). Since MaNGA is part of SDSS, we could easily cross-match their sample with ours. We used the additional kinematic parameters and more precise stellar masses provided in their catalogue for supplementary tests of our calibrations.

The value-added catalogue of Simard et al. (2011) contains Sersic-profile fits based on SDSS DR7 data (Abazajian et al. 2009) for 1 123 718 galaxies. We used their data for additional tests of our calibrations, but since we could not improve our calibrations with them, their impact on our analysis was minimal.

We found it useful to supplement the SDSS data with data from the 2MRS (Huchra et al. 2012), which was a spectroscopic follow-up to 2MASS (Skrutskie et al. 2006), in order to compensate for the saturation bias of the SDSS spectroscopic sample. Therefore, we included 43 533 galaxies from 2MRS with their 2MASS magnitudes (J , H , and K_S) and redshifts into our database. We cross-matched them with our complete SDSS sample and found that 5 890 galaxies were identified⁴ within the spectroscopic data of both surveys. We used these galaxies to calibrate the colour transformation (see Appendix D) and thereby calculate SDSS magnitudes for all 2MRS galaxies. Excluding the galaxies which were detected in both surveys, we found that 8 948 galaxies of 2MRS lie either in or within one degree of the SDSS spectroscopic footprint. We added these galaxies to our main sample, which was then used as a basis for our group catalogue.

Since the cosmological parameters of the first run of the Millennium simulation (Springel et al. 2005) are slightly outdated (Planck Collaboration et al. 2015; Suzuki et al. 2012), we decided to use its re-run by Guo et al. (2013), which assumed the cosmological parameters found by WMAP7 (Komatsu et al. 2011). The

re-run also provides semi-analytical galaxy models based on Guo et al. (2011), which we used to build mock-catalogues for the calibration of our group finder algorithm. We selected every galaxy with an absolute magnitude brighter than -15 mag in the i band from all snapshots between 61 (corresponding to redshift 0) and 46 (corresponding to redshift 0.5086). For these simulated galaxies, we gathered the parameters listed in Appendix A4. Each snapshot contains more than 10 million objects from which we selected the galaxies to construct our mock-catalogues.

In addition to all the data, which we required to calibrate and apply the fundamental plane, we also obtained various datasets using other distance indicators to test our own calibrations. Those include the catalogue of 740 Supernovae Type Ia distances by Betoule et al. (2014), the 56 124 distance measurements using the Tully-Fisher relation found in the latest version of the NASA/IPAC Extragalactic Database, and the distance measurements using various methods for 17 669 galaxies collected by the CosmicFlows project (Tully et al. 2016).

3 METHOD

3.1 Mock catalogues

The first step in building a group catalogue is to ensure that the group finder algorithm is well calibrated for the dataset it is applied on. The SDSS/BOSS data we used is the product of a series of selection criteria, which define the sparsity of the sample and thereby the optimal linking lengths of our FoF algorithm. To this end, we created a series of mock catalogues based on the data we obtained from the WMAP7 re-run of the Millennium simulation (Guo et al. 2013).

We built a set of (mostly) independent mock-catalogues from the available data. To this end, we decided to treat every snapshot independently as a representation of its particular redshift range. Each snapshot is a cube of a side length of $500/h$ Mpc. We calculated that it is possible to create 4 slices with no overlap at the lower redshifts and only limited overlap at the higher redshifts from each snapshot, if applying the following procedure. We defined centres for each slice at the following co-moving Cartesian coordinates: ($100/h$ Mpc, $250/h$ Mpc, $250/h$ Mpc), ($200/h$ Mpc, $250/h$ Mpc, $250/h$ Mpc), ($300/h$ Mpc, $250/h$ Mpc, $250/h$ Mpc), and ($400/h$ Mpc, $250/h$ Mpc, $250/h$ Mpc). Then we rescaled each snapshot to physical units. We call the redshifts corresponding to the time at which the snapshots were taken, the central redshift. We defined upper and lower limits for the redshift range associated with each snapshot by taking the average value between the central redshifts of two neighbouring snapshots. Then we translated the central redshift as well as the upper and lower limits to co-moving distances. Our virtual observer is located at a point, which is the co-moving distance of the central redshift (in the negative x -direction) away from the centre of each slice. All galaxies closer than the lower redshift limit (as a co-moving distance) from the virtual observer were removed from that slice, as well as all galaxies further away than the upper redshift limit. The resulting four slices only share a few galaxies with each other (especially considering the magnitude and colour-cuts introduced in the next step). We repeated the entire procedure in the y - and z -direction as well and end up with 12 largely independent slices for each snapshot.

Before we could introduce the SDSS/BOSS selection effects into our mock-catalogues, we had to obtain the redshift dependence of the uncertainties of the observed magnitudes in SDSS. To this end, we made use of the error-bars of the Petrosian magnitudes supplied by the catalogues. We split them into redshift bins, calculated

⁴ Using a tolerance of 10 arcseconds of angular separation and 300 km/s in radial velocity.

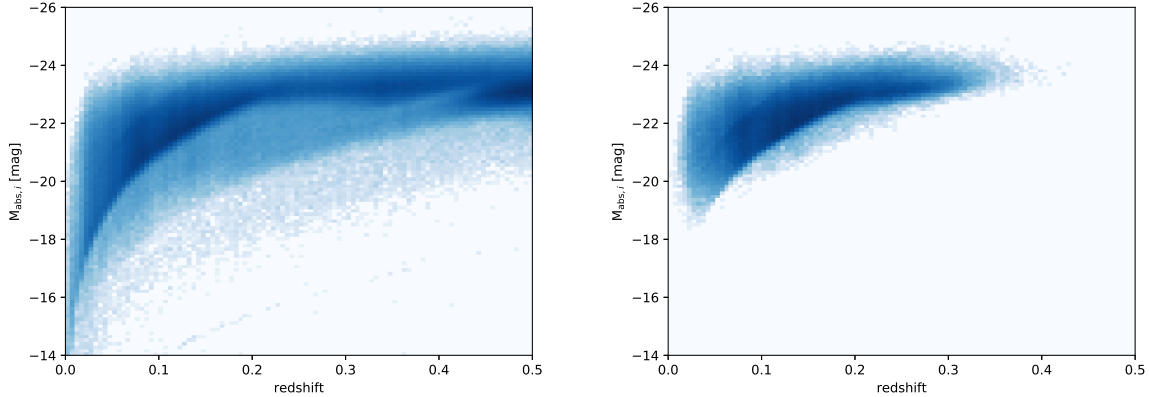


Figure 1. Redshift-absolute magnitude distribution of our samples. Left panel: the initial galaxy sample used for the group finder (SDSS/BOSS only). Right panel: initial early-type galaxy sample. The bluish heatmap represent the relative number densities of galaxies with dark blue tones indicating higher numbers.

the median, and did a simple interpolation between the bins. In the next step, we calculated the impact of the peculiar motions on the mock data.

$$z_{\text{real}} = \left((1 + z_{\text{cosmo}}) \cdot \left(1 + \frac{-v_{\text{pec}} \cdot n_{\text{view}}}{c} \right) \right) - 1 \quad (2)$$

While we could simply transform the co-moving distance to the virtual observer into a cosmological redshift z_{cosmo} , we had to take into account the peculiar motions of galaxies to obtain the ‘real’ redshift z_{real} . This is not the true observed redshift, since we still had to factor in the error of the redshift observation itself, which is done in Equation 4. v_{pec} denotes the vector of the peculiar motions from the Millennium simulation, n_{view} the unit-vector of the line-of-sight from the virtual observer to the galaxy, and c is the speed of light.

$$m_{\text{app,mock}} = M_{\text{abs,mill}} + \Delta m(z_{\text{cosmo}}) \cdot \mathfrak{G} + K(z_{\text{real}}) + 5 \cdot \log_{10}(D_L(z_{\text{cosmo}})/\text{pc}) - 5 \quad (3)$$

The apparent magnitude $m_{\text{app,mock}}$ of the galaxies in our mock-catalogues was obtained from the absolute magnitude $M_{\text{abs,mill}}$ found in the Millennium simulation by adding the observational error Δm of the magnitudes, the K-correction K , and the distance modulus, which is derived from the luminosity distances D_L . We use the symbol \mathfrak{G} to indicate a random Gaussian noise with a standard deviation σ of 1. Naturally, these corrections were applied to all magnitudes in all bands.

$$z_{\text{obs}} = ((1 + z_{\text{real}}) \cdot (1 + \Delta z \cdot \mathfrak{G})) - 1 \quad (4)$$

The actually observed redshift z_{obs} is obtained by considering the measurement error Δz of redshifts for the real redshifts z_{real} . In the next step, we applied the selection criteria for the various SDSS and BOSS samples on our mock-data. We considered the magnitude limit and saturation bias for the SDSS main galaxy sample, the colour, magnitude, and redshift cuts for the SDSS LRG low- z and SDSS LRG high- z samples, the colour and magnitude cuts for the BOSS low- z , BOSS CMASS and BOSS CMASSsparse samples, the main Quasar sample, and the magnitude limits of the 2MRS sample. Afterwards, we merged the various samples in each of our slices.

By directly applying the SDSS selection criteria on the mock-catalogues, which are using the semi-analytic galaxy models of Guo

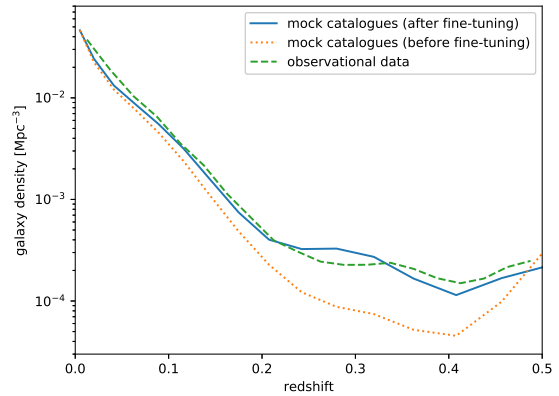


Figure 2. Galaxy density as a function of redshift in observational data and the mock catalogues.

et al. (2011), we found that the galaxy densities do not match and are not even reasonably near the values derived from observations (see Figure 2). We found a notable dearth of galaxies (by almost an order of magnitude) between a redshifts 0.2 and 0.45. Therefore, we had to fine-tune the selection criteria by adding some tolerances until we got the galaxy density in the mock catalogues reasonably close to the observed values across the entire redshift range. In particular, we allowed for an about 0.2 mag wider range for all magnitude limits and colour-cuts applied to select the various SDSS samples. After the fine-tuning, we combined all pairs of non-neighbouring slices (with each slice set to be pointing at opposite directions on the virtual sky) into our set of 6 mock catalogues for all of our 16 snapshots.

3.2 Group finder algorithm

In the next step, we ran our group finder algorithm on these mock catalogues to obtain the optimal linking lengths. Our version of the friends-of-friends approach follows Duarte & Mamon (2014), who pre-grid the data before running the nearest neighbour search to improve efficiency. We also used the *fofID* number from the Mil-

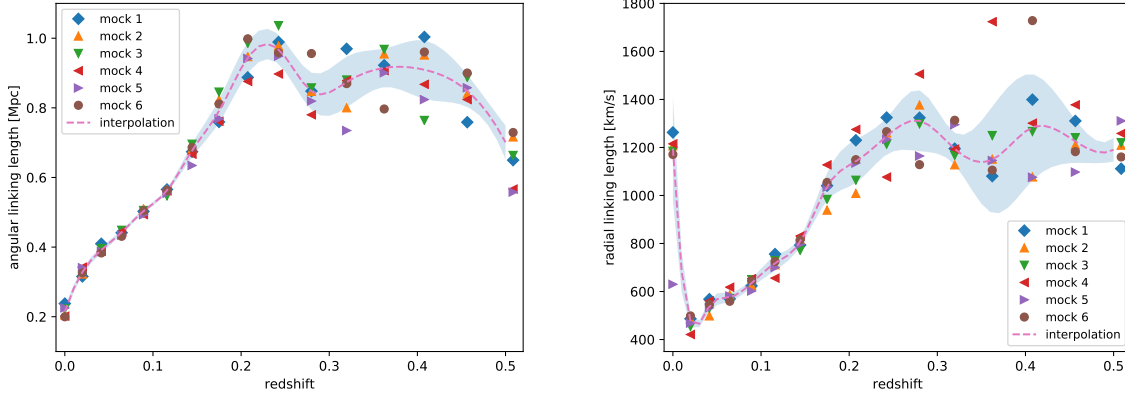


Figure 3. Optimized linking lengths used for our group finder algorithm. Left panel: angular linking lengths. Right panel: radial linking lengths. The various shapes mark optimal values derived from the different mock catalogues, the dashed-blue line indicates the interpolation we used in our group finder algorithm, with the blue shaded area highlighting the uncertainty.

lennium Run database to assemble groups which lie in the same dark matter halo. These halo-based groups are used as the comparison sample for identification of the best linking length for FoF in a given snapshot. We follow Robotham et al. (2011), and match groups between the FoF and halo-based catalogues according to a cost function based on bijective matches between groups in each catalogue. The cost function is based on matched groups that share at least 50% of their galaxies, and the group ‘purity’, see Equations 9-15 in Robotham et al. (2011). After obtaining the optimal values for all of our mock catalogues, we calculated the median of the optimal linking lengths of each mock catalogue for every snapshot (see Figure 3). The effects of the different samples are clearly visible in the linking lengths. At the lowest redshift bin, the saturation bias causes a larger linking length than for magnitude limited part of the SDSS main galaxy sample. There is a consistent rise in the linking lengths with redshift, which reaches a plateau once the more volume-limited samples such as the LRG and CMASS samples start to dominate. When comparing the scatter between the linking lengths of the individual mock catalogues to the galaxy densities of Figure 2, we see that it noticeably increases once the sample gets sparser. We used cubic splines to interpolate between the different redshifts and applied these interpolations in our group finder.

Before we could use our group finder on SDSS data, we had to filter and properly calibrate the observational data first.

$$m_{\text{extcor}} = m_{\text{obs}} - A_{\text{Schlegel}}. \quad (5)$$

We corrected the SDSS⁵ magnitudes m_{obs} for galactic extinction A_{Schlegel} according to the Schlegel maps (Schlegel et al. 1998) to obtain the extinction-corrected magnitude m_{extcor} . In the case of the galaxies, which were only in the 2MRS sample, we used the extrapolated SDSS magnitudes based on a fit using the H- K_s and J-H colours and the K_s band magnitudes instead. This fit was calibrated using galaxies in both surveys and the details of this method are explained in Appendix D.

$$K(z, m_{f_1} - m_{f_2}) = \sum_{i,j} B_{ij} z^i (m_{f_1} - m_{f_2})^j \quad (6)$$

⁵ We use the index *obs* to mark observational parameters directly taken from the SDSS database.

$$m_{\text{app}} = m_{\text{extcor}} - K(z_{\text{obs}}, m_{f_1} - m_{f_2}). \quad (7)$$

Afterwards, we applied a K-correction $K(z_{\text{obs}}, m_{f_1} - m_{f_2})$ to the extinction-corrected magnitudes m_{extcor} . We used the K-correction of Chilingarian et al. (2010), with updated coefficients from Saulder et al. (2013). $m_{f_1} - m_{f_2}$ denotes any suitable colour and z_{obs} the observed redshift directly from the SDSS pipeline. We used the following combinations: g band: g-r colour, r band: g-r colour, i band: g-i colour, z-band: g-z colour, J band: J- K_s colour, H band: H- K_s colour, and K_s band: J- K_s colour.

We also transformed all redshifts to the CMB-rest frame. With the CMB-redshifts z_{cmb} , we calculated the angular diameter distances D_A and the luminosity distances D_L . Using the distance modulus, we calculated the absolute magnitude M_{abs} and derived the luminosity L in solar units using the absolute magnitude of the sun (Willmer 2018) $M_{\text{abs},\odot}$.

$$v_{\text{rad}} = c \cdot \frac{(1 + z_{\text{cmb}})^2 - 1}{(1 + z_{\text{cmb}})^2 + 1} \quad (8)$$

Since our radial linking length was calibrated in km/s, we also transformed the redshifts into radial velocities v_{rad} for every galaxy.

To remove potentially problematic objects, we removed all galaxies with an absolute magnitude brighter than -30 mag and fainter than -15 mag in the i band. Furthermore, all objects with a g-i colour of more than 3 mag or less than -2 mag were excluded from the sample. Since we did not want to have any galaxies outside the calibrated range of our group finder, we removed all objects with a redshift z_{cmb} lower than zero and higher than 0.5. These cuts reduced our sample to 1 480 600 galaxies.

$$l_{\alpha} = \text{atan} \left(\frac{l_b}{D_A} \right) \quad (9)$$

When we ran our FoF group finder, we could take the radial linking length l_R directly and compare it with the radial velocity v_{rad} . However, we had to transform our angular linking length l_b from physical units to angles l_{α} .

Besides just assigning group memberships, our group finder calculated the several parameters for every group that it detected using the methods thoroughly tested in Robotham et al. (2011) and discussed again for a similar group finder algorithm in Saulder et al.

(2016). The radial group centre was calculated by taking the median of the redshifts of all group members. The projected group centre was found by using the centre of light of the group members and iteratively removing the members with largest angular separation. The projected group radius was defined as the distance from that projected group centre in which 50% of the group members are located.

We calculated group velocity dispersions using the gapper estimator of Beers et al. (1990) including the modification of Eke et al. (2004).

$$\sigma_{\text{gap}} = \frac{\pi}{N_{\text{fof}}(N_{\text{fof}} - 1)} \sum_{i=1}^{N_{\text{fof}}-1} w_i g_i, \quad (10)$$

$$w_i = i \cdot (N_{\text{fof}} - i), \quad (11)$$

$$g_i = v_{i+1} - v_i, \quad (12)$$

$$\frac{v_i}{c} = \frac{(1 + z_{\text{obs},i})^2 - 1}{(1 + z_{\text{obs},i})^2 + 1}, \quad (13)$$

$$\sigma_{\text{group}} = \sqrt{\frac{N_{\text{fof}}}{N_{\text{fof}} - 1} \sigma_{\text{gap}}^2 - \sigma_{\text{err}}^2}. \quad (14)$$

The gapper velocity dispersion σ_{gap} of a group with N_{fof} member was calculated by summing up the product of the weights w_i and the radial velocity gaps g_i for all its members. It was essential that the radial velocities v_i were ordered for this approach, which we assured by applying a simple sorting algorithm for each group. The radial velocities v_i were calculated using the observed redshifts $z_{\text{obs},i}$. The group velocity dispersion σ_{group} also took into account the measurement errors of the redshift determination σ_{err} , which were 30 km/s for SDSS, 65 km/s for BOSS, and ~ 32 km/s for 2MRS. In the case that the obtained group velocity dispersion was lower than the measurement errors of the redshift determination, we set them to their corresponding σ_{err} .

The observed group luminosity is merely the sum of the i band luminosities of all its detected members.

3.3 Basic calibrations for early-type galaxies

Most parameters needed to get to the different fundamental plane calibrations are the same. The extinction correction and the K-correction were already presented in Equation 5 and Equation 6, respectively. Besides these two corrections, the apparent magnitudes are typically also corrected for evolutionary effects. As illustrated by the dearth of bright galaxies at very low redshifts in Figure 1, the saturation bias of SDSS spectroscopy removes all galaxies from the main galaxy sample with apparent magnitudes brighter than 15 mag in the g and r band and brighter than 14.5 mag in the i band. As illustrated in Figure 4, the saturation bias is different and poorly defined for the LRG sample of SDSS. The BOSS low-z sample, which also contributed galaxies to our catalogue, suffers from a saturation bias for galaxies brighter than 16 mag in the r band, but there are other galaxies observed with BOSS fibres that are not affected by this bias. At higher redshifts, the sample of early-type galaxies gets increasingly sparse, on the one hand due to Malmquist bias, which removes the intrinsically faintest galaxies in magnitude-limited surveys, and on the other hand the light profiles become increasing

PSF-like, which means that the likelihood for a de Vaucouleurs-profile as calculated by the SDSS pipeline shrinks correspondingly. Consequently, this does not allow for easy classification according to our criteria (see Appendix A2).

$$m_{\text{app,evcor}} = m_{\text{app}} + Q \cdot z_{\text{group}} \quad (15)$$

To obtain the evolution corrected magnitude $m_{\text{app,evcor}}$, we took advantage of our group catalogue and used the group redshift z_{group} , which should be barely affected by the finger-of-god effects in clusters. All derivative quantities using the apparent magnitude were calculated in two ways, one using the evolution corrected magnitude $m_{\text{app,evcor}}$ and one using the uncorrected apparent magnitude m_{app} . The evolution correction parameter Q is obtained by finding a constant number density for the brightest galaxies within the redshift range for which our sample of these galaxies is the most complete. We estimated the redshift range in which our early-type galaxy sample is complete for galaxies brighter than -23.5 mag in the z band to be between 0.07 and 0.25. Within this redshift range, we calculated the mean separation to the five nearest neighbours for all galaxies brighter than -23.5 mag after applying the evolution correction parameter Q and split them into 0.01 wide redshift intervals. We varied Q between 0 and 2 mag/z and found that the optimal value that preserves the mean separation (hence indirectly the number density) of the brightest objects in the sample is 0.71 mag/z. This value is slightly lower than the evolution corrections found in Bernardi et al. (2003) and Saulder et al. (2013). We argue that this might be due to the fact that we only focused on the brightest galaxies of our sample. However, this is well motivated since these are the only galaxies that we are able to detect at higher redshifts, where the evolution correction becomes increasingly important.

We also corrected the sizes and velocity dispersions for evolutionary effects. To this end, we used the corrections provided by Beifiori et al. (2014).

$$r_{\text{cor}} = r_{\text{sdss}} (1 + z_{\text{group}})^{-\beta} \quad (16)$$

$$\sigma_{\text{cor}} = \sigma_{\text{sdss}} (1 + z_{\text{group}})^{-\gamma} \quad (17)$$

The corrected sizes r_{cor} and velocity dispersions σ_{cor} are rescaled from the observed parameters directly from the SDSS pipeline r_{sdss} and σ_{sdss} . We took the values of the scaling coefficients β and γ directly from Beifiori et al. (2014), which were -0.49 ± 0.26 and 0.12 ± 0.02 respectively.

$$r_{\text{circ}} = r_{\text{cor}} \sqrt{q_{b/a}} \quad (18)$$

Following Bernardi et al. (2003), we circularized the evolution corrected angular radius r_{cor} using the minor semi-axis to major semi-axis ratio $q_{b/a}$ to obtain the circularized radii r_{circ} , which is more reliable quantity to compare galaxies of different shapes.

Because SDSS/BOSS uses fixed size fibres, we had to correct for the fact that at different distances different fractions of the galaxies are covered by that fibre. Based on the work of Jorgensen et al. (1995) and Wegner et al. (1999), we used the following equation:

$$\sigma_0 = \sigma_{\text{cor}} \cdot \left(\frac{r_{\text{fiber}}}{r_{\text{circ}}/8} \right)^{0.04} \quad (19)$$

The radius r_{fiber} of the SDSS fibres used to be 1.5 arcseconds, but with the upgrade (Ahn et al. 2012) done for BOSS, new smaller fibres were installed. These fibres only have a radius of 1 arcsecond. SDSS marks whether a spectroscopic measurement was obtained

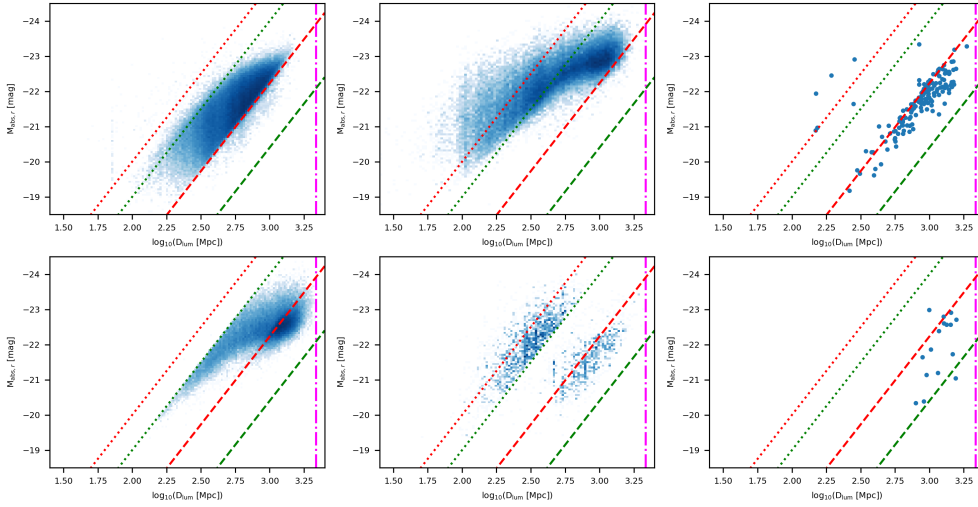


Figure 4. Our sample of early-type galaxies used for the fundamental plane calibrations split into the different subsamples. Top-left panel: SDSS main galaxy sample only; top-centre panel: SDSS LRG sample; top-right panel: other samples observed with SDSS fibres; bottom-left panel: BOSS low-z sample; bottom-centre panel: other samples observed with BOSS fibres, but no flags sets; bottom-right panel: CMASS sample (regular CMASS and CMASS sparse combined). Red dotted line: official saturation limit in SDSS; green dotted line: official saturation limit in BOSS; red dashed line: limiting magnitude of the SDSS main galaxy sample; green dashed line: limiting magnitude for the BOSS low-z galaxy sample; magenta dashed-dotted line: redshift-limit of our early-type galaxy sample.

using the SDSS fibres or the BOSS fibres. σ_0 denotes the corrected central velocity dispersion, while σ_{cor} denotes the evolution corrected central velocity dispersion. We also tested the slightly modified version of Equation 19 from Cappellari et al. (2006) and found that the velocity dispersions obtained from their method yields a marginally higher scatter for the fundamental plane.

$$R_e = D_A(z_{\text{group}}) \cdot \tan(r_{\text{circ}}) \quad (20)$$

Using basic trigonometry, one can calculate the physical radii R_e of galaxies using their angular diameter distances D_A (derived using the median group redshifts z_{group}) and circularized radii r_{circ} . When we refer to redshift-based distances throughout this paper, we mean distances derived using the redshift-distance relation with the assumed cosmology of this paper and the median group redshifts.

$$\mu_e = m_{\text{app}} + 2.5 \cdot \log_{10} \left(2\pi \cdot r_{\text{circ}}^2 \right) - 10 \cdot \log_{10} (1 + z_{\text{group}}) \quad (21)$$

When calculating the surface brightness μ_e , one has to include a correction for the cosmological dimming of surface brightnesses, which is proportional to $(1+z)^4$ in any Friedmann-Lemaître-Robertson-Walker metric-based universe (Tolman 1930; Hubble & Tolman 1935; Sandage & Perlmutter 1990a,b, 1991; Pahre et al. 1996).

Before we could fit any fundamental plane, we should further clean our sample, because we had some additional parameters to work with after doing the basic calibrations. We keep only galaxies that fulfil a set of criteria and cuts listed in Appendix A3.

For technical reasons, we had to merge the stellar masses provided directly by the SDSS database with the updated dataset⁶ for galaxies observed with the new BOSS fibres. For a few (~ 2000)

galaxies of our initial sample of early-type galaxies, stellar masses were not provided and these galaxies were also removed from the sample.

Additionally, we iteratively removed all $5\text{-}\sigma$ outliers of the two main fundamental plane calibrations presented in this paper (see the next three subsections). To this end, we used a Levenberg-Marquardt algorithm and least squares using a $5\text{-}\sigma$ clipping as implemented in ASTROPY (Astropy Collaboration et al. 2013; Price-Whelan et al. 2018).

After applying all these filters, we ended up with the final sample of 317 285 early-type galaxies used for all our fundamental plane calibrations. The main contributions to our early-type galaxy sample are the SDSS main galaxy sample with 181 719 galaxies, the BOSS low-z sample with 71 311 galaxies, and the SDSS LRG sample with 60 505 galaxies. Additionally, there are minor contributions from other samples obtained using the SDSS fibres (162 galaxies), the CMASS samples (16 galaxies), and a poorly defined subsample obtained with the BOSS fibres, but no selection-flags set (3 579 galaxies). As illustrated in Figure 4, the selection criteria for most (aside from the SDSS main galaxy sample) of the different subsample are non-trivial.

3.4 Fitting the traditional fundamental plane

Since we primarily intend to use the fundamental plane as a distance indicator, we aimed to minimize the scatter in the physical radii R_e . This can be best achieved using a direct fit (Sheth & Bernardi 2012) applied on Equation 1. By inverting Equation 20, we could use the predicted physical radii for given surface brightnesses and central velocity dispersions to derive the angular diameter distances for the traditional fundamental plane by comparing it to the observed angular radii. We used our group catalogue again on the resulting

⁶ https://www.sdss.org/DR15/spectro/galaxy_portsmouth/

fundamental plane distances and calculated the median fundamental plane distance to every detected group. Thereby, we improved the distance estimates to all groups containing more than one early-type galaxy by taking the average of the fundamental plane distances to all members and thereby reducing the statistical uncertainty.

3.5 Distances corrected for systematic residuals

We intentionally did not apply a correction for various selection effects (e.g. Malmquist bias, saturation bias, and colour-cuts). We attempted to consider these effects using the method of volume-weights (Sheth & Bernardi 2012; Saulder et al. 2013), but due to various sub-samples of SDSS/BOSS contributing to our sample and their sometimes difficult to reproduce selection criteria and affected cross-correlations with the main parameters of the fundamental plane, we were not able to get useful results. Hence, we considered the methods used in 6dFGSv (Magoulas et al. 2012; Howlett et al. 2017; Qin et al. 2018). While a fully Bayesian approach to correct for the biases after the traditional fundamental plane calibrations would run into the same problems as the volume-weights due to insufficiently well-defined selection criteria of several subsamples, we settled for a slightly simpler but effective model inspired by that method.

The distances obtained using the traditional fundamental plane following the method of the previous section are systematically biased due to various selection effects (illustrated in Figure 5 for the strong dependence on the absolute magnitude of the fundamental plane residuals). To correct for this, we measured the average systematic offsets in the apparent magnitude-redshift plane within bins (see Figure 6). We choose this parametrization, because some of the selection effects create relatively clear cuts. We designed the bins to be one magnitude times 0.04 in redshift wide. We sampled at twice the resolution of the bins sizes, so that the data in each bin is partially shared with its neighbours. We then fit a fourth-order (second-order has notable problems for the faintest and brightest galaxies, third-order was off-set in the centre) two-dimensional polynomial to these bins and used it to obtain the correction function: $f_{\text{cor}}(m_{\text{app,cor}}, z_{\text{group}})$.

$$\log_{10}(R_{e,\text{cor}}) = a \cdot \log_{10}(\sigma_0) + b \cdot \mu_e + c \cdot f_{\text{cor}}(m_{\text{app,cor}}, z_{\text{group}}). \quad (22)$$

Using the correction function to obtain corrected sizes $R_{e,\text{cor}}$ for the fundamental plane galaxies and using them in turn to calculate distances, we were able to largely remove luminosity and redshift dependent biases and selection effects. As illustrated in Figure 6, our correction function can reproduce the mean residuals in the bin very well within the range of our galaxy sample. Beyond the range of our sample of early-type galaxies, the function is barely constrained, but also irrelevant for our analysis.

3.6 The expanded fundamental plane

The simplest way to reduce scatter in a relation is by adding additional terms (and thereby also free parameters) to account for previously unconsidered correlations.

$$\log_{10}(R_e) = a_{\text{exp}} \cdot \log_{10}(\sigma_0) + b_{\text{exp}} \cdot \mu_e + d_{\text{exp}} \cdot \log_{10}(M_*) + c_{\text{exp}}. \quad (23)$$

To distinguish the coefficients of the expanded fundamental plane from the coefficients of the traditional fundamental plane, we added

the index *exp* to the coefficients in Equation 23. When testing for systematic biases and studying the residuals of the fundamental plane, we found that for our specific SDSS-based sample that the single best expansions of the fundamental plane is the stellar mass M_* obtained by the Wisconsin method (Chen et al. 2012) using Maraston models (Maraston & Strömbäck 2011). We also tested other stellar mass estimates provided by SDSS such as the one based on Maraston et al. (2009), but found that the Wisconsin method yielded the best results for our applications.

4 RESULTS

4.1 Group catalogue

We used 1 473 971 galaxies from SDSS (Aguado et al. 2018) and 6 629 galaxies from 2MRS (Huchra et al. 2012) to create a group catalogue out to as far as a redshift of 0.5 while covering the 9 376 square degree footprint of the SDSS spectroscopic sample. The group catalogue was constructed using a Friends-of-Friends algorithm, for which we calibrated the linking length based on mock catalogues derived from the WMAP7 re-run of the Millennium simulation (Guo et al. 2013) and the selection criteria for the various samples that compose SDSS/BOSS and 2MRS, taking into account all significant biases. However, the direct implementation of the selection criteria yielded a far too low galaxy density (see Figure 2), which required us to fine-tune the sample selection for the mock catalogues. The colour cuts of the LRG, BOSS low-*z* and CMASS sample are especially sensitive to small systematic offsets between the semi-analytic galaxy models of Guo et al. (2011) and observations. The inclusion of 2MRS partially compensated the saturation bias of the SDSS spectroscopic sample by supplying redshifts to nearby bright galaxies. It assures that the brightest group galaxies are included, making sure the group centre is found correctly.

With our optimized FoF group finder algorithm, we detected 165 132 groups and 997 161 individual galaxies within our SDSS/BOSS/2MRS dataset consisting of 1 480 600 objects. This does not necessarily mean that all the individual galaxies that are not members of detected groups are isolated galaxies, but that due to Malmquist bias and other selection effects, we often only detected the brightest galaxy in many of these groups. We find 3 467 groups with ten or more members and 25 groups even contain more than a hundred galaxies. Naturally, the (apparently) richest groups are at lower redshifts (see Figure 7), which is expected since there the sample is the most complete, because it was derived from primarily magnitude-limited surveys. The majority of the saturation bias of SDSS was successfully corrected by the inclusion of 2MRS data. Overall, the group catalogue shows the expected properties, given the dataset used to create it. The complete group catalogue can be found in Tables B1 and B2.

The primary application of the group catalogue in this paper was to collapse the huge redshift space distortions (Finger of God effect) caused by the proper motions of galaxies in clusters and to be able to derive more accurate fundamental plane distances for rich clusters by combining the distances derived for different individual galaxies in said clusters. To be more specific, of our 318 149 early-type galaxies, 182 057 are individual galaxies and the remainder is located 75 822 different groups. Within these groups, 43 851 only contain one early-type galaxy for which we have fundamental plane distances. This leaves 31 971 groups hosting at least two early-type galaxies and 4 864 groups contain four or more early-type galaxies, which means that we could reduce the error of the

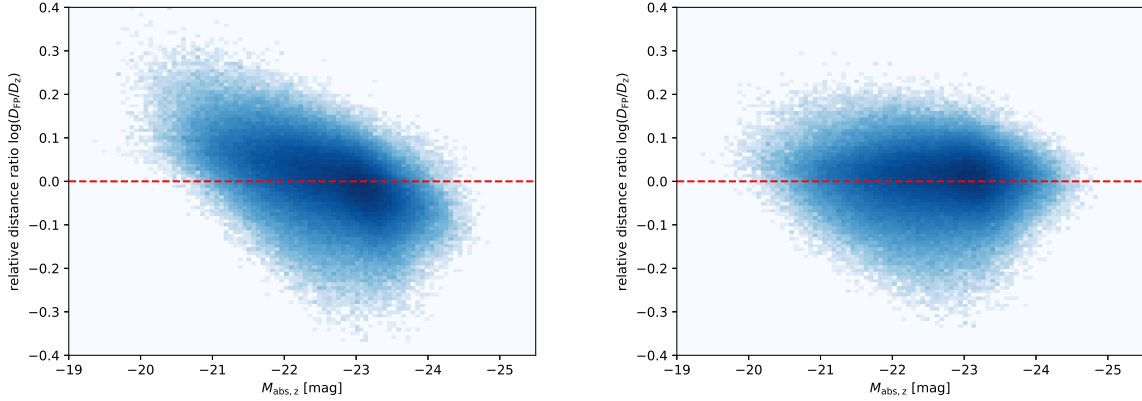


Figure 5. Ratio between the fundamental plane distance and redshift-based distance as a function of the absolute magnitude in the z band. Left panel: traditional fundamental plane distances without any corrections; right panel: fundamental plane distances corrected for selection effects.

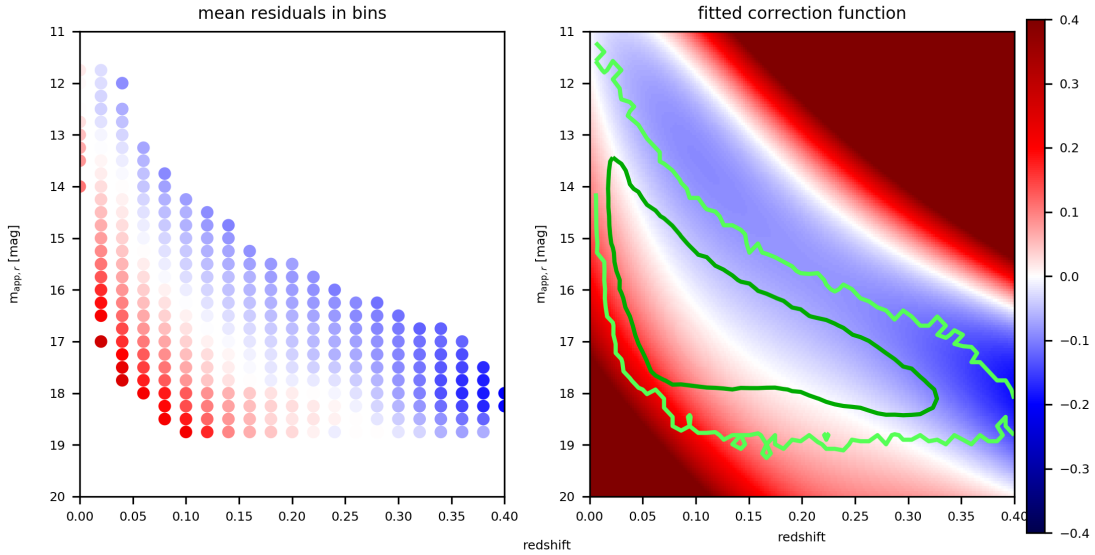


Figure 6. Effective correction of systematic residuals. Left panel: mean systematic residuals in each bin; right panel: fitted polynomial to correct for these systematic residuals. Red-white-blue colours: values of the residuals within the bin/at the point of the correction function; light green contour: distribution of the early-type galaxy sample; dark green contour: distribution of the most dense part of the early-type galaxy sample.

distance measurements by about a factor of two. By combining the redshift measurements of several cluster members, we were able to largely remove the scatter introduced by the virial motions in said clusters. Additionally, the combination of independent fundamental plane distance measurements to several early-type galaxies within these clusters, we were also able to reduce the scatter on the distance measurements, save for residual systematic uncertainties. 582 groups even host at least ten early-type galaxies resulting in even better distance estimates for them. Furthermore, the group catalogue allowed for a comparison of our results with Tully-Fisher relation distances and the distance from the CosmicFlows-3 sample.

With our catalogue, we reached beyond the group catalogue of Yang et al. (2007), which was limited by the SDSS DR7 spectroscopic sample and did not provide any groups at very low redshifts ($z < 0.05$). The RedMapper catalogue (Rykoff et al. 2014) also

excluded galaxies below a redshift of 0.08, but it has a bigger sample, since it also contains galaxies with only photometric redshifts. However, for the comparison with the Tully-Fisher relation and the CosmicFlows-3 dataset, nearby clusters are crucial, hence we could not just use the RedMapper catalogue. We also moved beyond the limited depth ($z < 0.1$) of the Saulder et al. (2016) catalogue, which is completed at the low redshift range. Thereby, our improved group catalogue presented in this paper provides the ideal properties for our application to improve the fundamental plane distance measurements and compare them to other distance indicators.

4.2 Traditional fundamental plane

We fitted the traditional fundamental plane using Equation 1 to our sample of 317 285 early-type galaxies. Thereby, we obtained

band	a	b	c	rms
g	0.889 ± 0.002	0.2772 ± 0.0002	-7.129 ± 0.006	0.0908
r	0.958 ± 0.001	0.2896 ± 0.0002	-7.311 ± 0.006	0.0871
i	0.986 ± 0.001	0.2944 ± 0.0002	-7.355 ± 0.005	0.0850
z	1.004 ± 0.001	0.2979 ± 0.0002	-7.371 ± 0.005	0.0833

Table 1. Coefficients of the traditional fundamental plane optimized for usage as a distance indicator for our SDSS/BOSS sample.

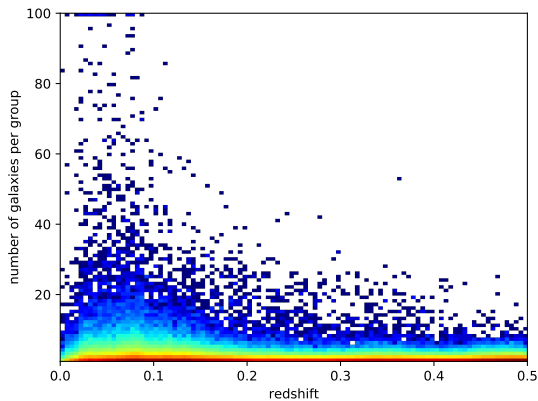


Figure 7. Richness of the detected groups as a function of the redshift. Groups with more than 100 members are mapped to 100 to keep this figure compact.

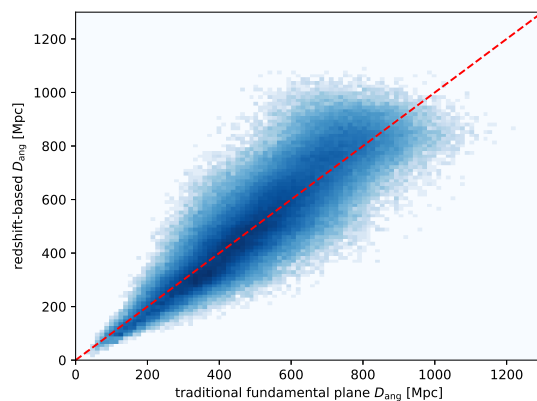


Figure 9. Traditional fundamental plane distance compared to the redshift based distances, which were used for calibration.

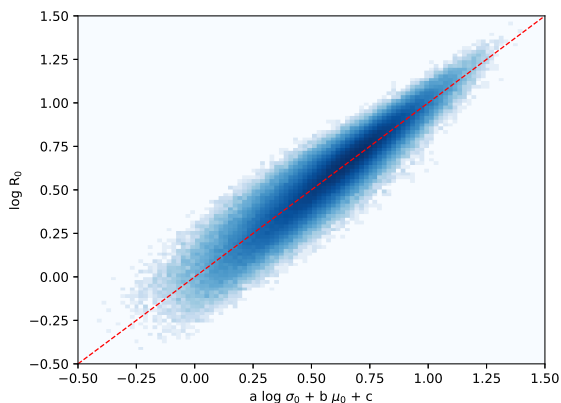


Figure 8. The traditional fundamental plane in z band, projected edge-on.

the coefficients and root-mean square listed in Table 1. The fit is illustrated in Figure 8. The complete catalogue of fundamental plane distances derived using this method can be found in Table B3. These calibrations were not corrected for any biases and selection effects yet, because of the various overlapping sample these effects and cross-correlations arising from them are extremely difficult to estimate. Hence, the hereby obtained coefficients are only to be used for the same SDSS/BOSS dataset, and not for any other galaxies without additional corrections. We discuss an effective correction for the distances obtained using these calibrations in the next section.

The root-mean square of the fundamental plane is smaller in the redder filters. Hence, we use the z band for our distance measurements. In Saulder et al. (2013), it was shown that a combination of

traditional fundamental plane distances from different filters would not improve the distance estimate beyond what one can reach in the band with the smallest root-mean square due to tight correlations of the fundamental plane parameters in between the different bands. We repeated this test with our data and could confirm their results. We find that the relative scatter of the traditional fundamental plane seems to slightly decrease (stays constant for absolute values after rising with distance at lower redshifts) for higher redshift galaxies, as illustrated in Figure 9. In the z band, we found a mean relative distance uncertainty of the fundamental plane of 18.4% when combining it with our group catalogue. The distance uncertainty without the group catalogue lies at 20.2%, which nicely illustrates the improvement achieved by combining the fundamental plane distances with our group catalogue. About 0.3 percentage points of this uncertainty can be attributed to systematic redshift bias, because of the hidden redshift dependences in the evolution corrections as well as the correction for the Tolman effect. When studying the residuals of the fundamental plane, we found a notable dependence on the galaxies' absolute magnitudes (see Figure 5). Distances to the intrinsically fainter early-type galaxies are systematically overestimated by almost a factor of two, and distances to the intrinsically brightest early-type galaxies are systematically underestimated. Considering the saturation bias of some of the SDSS spectroscopic sample as well as the Malmquist bias of the magnitude limited parts of the survey, this causes a systematic overestimation of the distances to the most nearby objects and an underestimations of the distances to the farthest galaxies. A closer investigation of the biases and selection effects lead us directly to the effective model discussed in the next section as well as to the expanded fundamental plane.

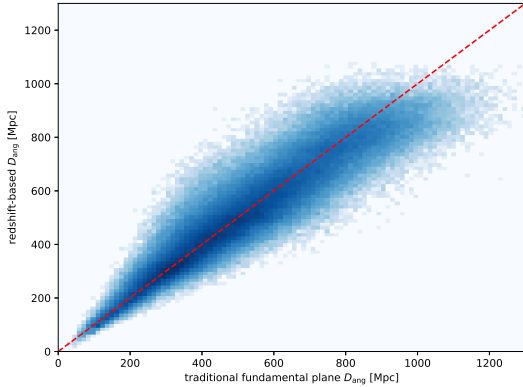


Figure 10. Corrected fundamental plane distance compared to the redshift-based distances.

4.3 Distances corrected for systematic residuals

The dominant bias of affecting the distances obtained using the traditional fundamental plane correlates with the absolute magnitude of the respective galaxies (see Figure 5). Since these absolute magnitudes were calculated using the redshift-based distances, we could not directly use them to remove the residuals created by them. In fact, the selection effects and cut-offs are best constrained in the redshift-apparent magnitude plane. Therefore, by applying the method described in Section 3.5, we mapped the average residuals in this plane within bins and fitted a polynomial to obtain a correction function (see Figure 6). The correction function is well constrained with the range of our sample, which was sufficient for our applications. Using Equation 22, we adjusted the predicted radii of the early-type galaxies for these systematic residuals.

We used these corrected radii to obtain distances (see Figure 10) to the early-type galaxies in our sample, which are provided in Table B4. Aside from removing systematic effects created by the various selection criteria, this method also reduces the overall scatter of the fundamental plane distances to 15.9% without and 14.5% with the group catalogue. Since the correction function by its very definition is redshift dependent, one might suspect that the redshift-dependent systematics might increase, but they actually slightly decrease to 0.2 percentage points of the scatter.

4.4 The expanded fundamental plane

Here, we present the results of our calibration of the expanded fundamental plane, which was explained in Section 3.6. We start by examining the short-comings of the traditional fundamental plane, which motivated us to proceed with this alternative calibration.

The residuals of the traditional fundamental plane are strongly correlated with the estimated stellar masses of the galaxies (see Figure 11). Despite the notable scatter of the stellar masses of the spectro-photometric Wisconsin method (Chen et al. 2012) using Maraston models (Maraston & Strömbäck 2011), one can clearly see a systematic effect. It becomes more striking, when one uses the higher quality stellar masses for MaNGA galaxies (Graham et al. 2018). As already illustrated in Figure 5, the residuals also correlated with the absolute magnitudes, which is expected, since the stellar mass and the (redder) absolute magnitudes also correlate with each other. The simplest way to incorporate this in the fundamental

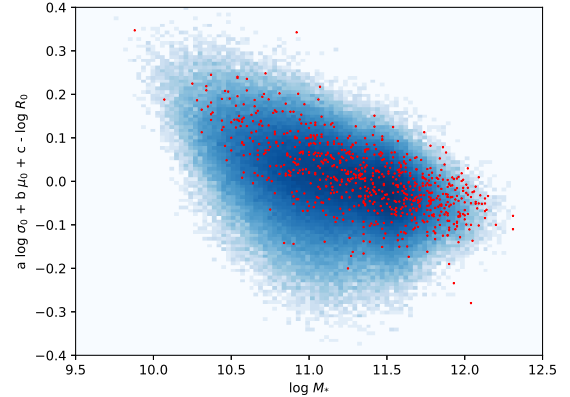


Figure 11. Dependence of the residuals of the traditional fundamental plane on the stellar mass based on SDSS data (blueish cloud) and MaNGA data (tiny red stars).

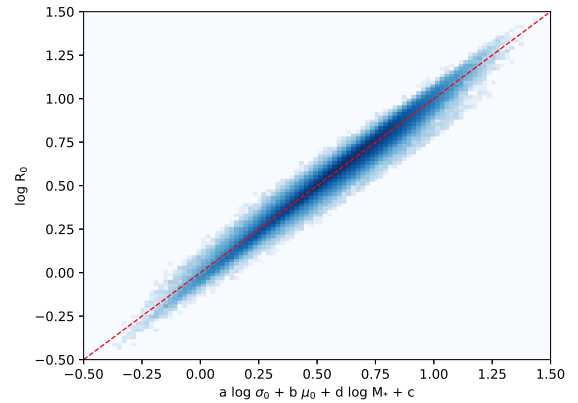


Figure 12. The expanded fundamental plane in z band, projected edge-on.

plane calibrations is by expanding with a term proportional to the logarithm of the stellar mass.

By fitting Equation 23 to the data, we obtained the values listed in Table 2 for the coefficients of the expanded fundamental plane. As illustrated in Figure 12, this fit is notably tighter than for the traditional fundamental plane (see Figure 8) and it reduced the uncertainty of the individual fundamental plane distances to 9.6% and to 9.0% when also applying the group catalogue to further reduce the scatter. This is a significant improvement in the distance estimates (see Figure 13). However an explicit systematic redshift dependence gets more complex. In contrast to the redshift dependent systematics of the traditional fundamental plane, the magnitude of the systematics for the expanded fundamental plane correlates with the redshift itself as well. In the case of nearby galaxies (redshifts below 0.03), we have a contribution of 1.7% redshift dependent systematic bias. It continuously shrinks to almost zero (0.07%) for redshifts of 0.2 and higher. On average for the entire sample, we find a contribution to the overall scatter due to systematic redshift bias is with 0.4 percentage points of the same magnitude as the traditional fundamental plane. This systematic bias arose from a combination of the redshift dependence of the evolution correction,

band	a_{exp}	b_{exp}	d_{exp}	c_{exp}	rms
g	-0.121 ± 0.001	0.1929 ± 0.0001	0.4100 ± 0.0004	-7.628 ± 0.003	0.0454
r	-0.043 ± 0.001	0.1971 ± 0.0001	0.4022 ± 0.0004	-7.657 ± 0.003	0.0424
i	-0.002 ± 0.001	0.2023 ± 0.0001	0.3930 ± 0.0004	-7.681 ± 0.003	0.0404
z	0.022 ± 0.001	0.2064 ± 0.0001	0.3840 ± 0.0004	-7.660 ± 0.003	0.0403

Table 2. Coefficients of the expanded fundamental plane optimized for usage as a distance indicator for our SDSS/BOSS sample.

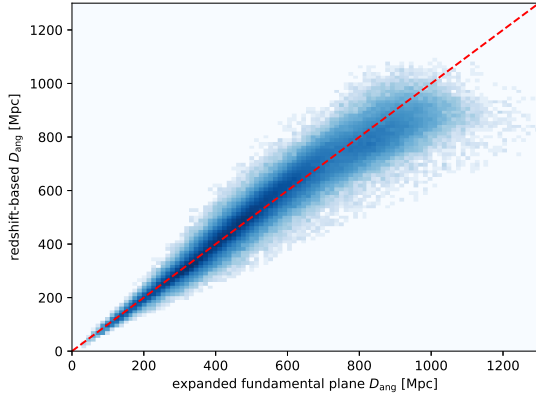


Figure 13. Expanded fundamental plane distance compared to the redshift based distances, which were used for calibration.

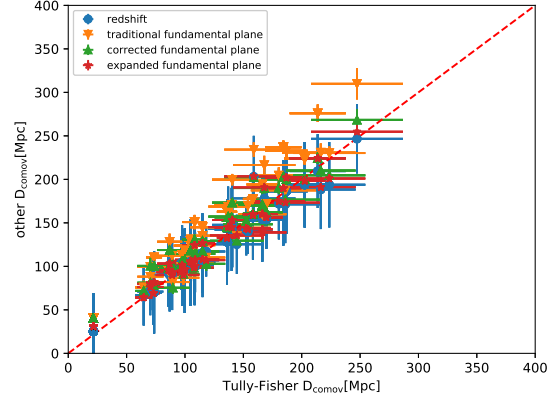


Figure 15. Comparison between Tully-Fisher relation distances and various fundamental plane and redshift-based distances for groups that host at least three late-type and at least three early-type galaxies.

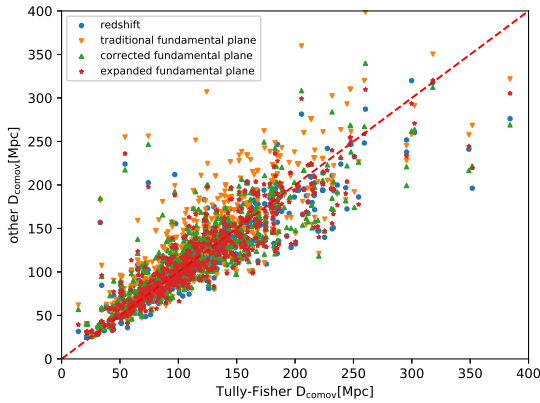


Figure 14. Comparison between Tully-Fisher relation distances and various fundamental plane and redshift-based distances. Error bars were omitted in this figure to avoid overcrowding, but they were of about the same size as in Figure 15.

the correction for the Tolman effect, and the additional systematics caused by the use of the stellar masses. We provide a complete catalogue of expanded fundamental distances derived using this method in Table B5.

4.5 Comparison with Tully-Fisher relation data

We cross-matched galaxies with known Tully-Fisher relation distances within the NASA/IPAC Extragalactic Database with our group catalogue and found 4 481 objects. To be more precise, we found 20 900 Tully-Fisher relation based distance measurements for

4 481 unique galaxies. As a consistency check, we compared the Tully-Fisher distances to the redshift-based distances and found an overall scatter of 27.6% (and 23.5% for groups) hosting them, which is about the magnitude expected for it, considering the database contains distances from various sources. Since the Tully-Fisher relation only works for late-type galaxies and the fundamental plane only works for early-type galaxies, we do not have a direct overlap between the distance indicators. Hence we had to take advantage of our group catalogue. We selected every cluster that had at least one galaxy with Tully-Fisher relation distances and at least one galaxy with fundamental plane distances. 539 groups in our dataset fulfilled this requirement. Also illustrated in Figure 14, we find poor agreement with the traditional fundamental plane (41.7% error on average), which is mostly because the traditional fundamental plane tends to overestimate distances due to the saturation bias of SDSS the parameters being optimized for the bright galaxies due to our sample selection. The brightest galaxies are missing in the overlapping region between our fundamental plane distances and the Tully-Fisher relation distances. After correcting for the systematic biases of the traditional fundamental plane, we still found a sizeable scatter of 37.0% when comparing them to Tully-Fisher relation data. With our expanded fundamental plane, which also considers the stellar masses of the galaxies, we obtained a 31.3% scatter between the Tully-Fisher relation distances and the distances derived from the expanded fundamental plane. These values are marginally better than the scatter between the redshift-based distances and the Tully-Fisher relation distances of 29.4%. This subsample is still plagued by occasional interlopers due to imperfections of the group catalogue.

When looking at richer groups, that contain at least three galaxies for which we have Tully-Fisher relation distances in our database and at least three galaxies for which we derived fundamental plane

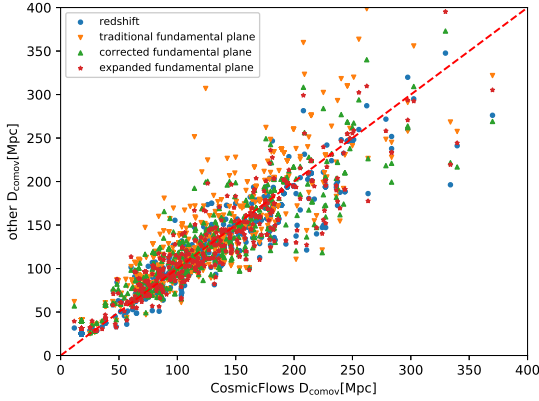


Figure 16. Comparison between CosmicFlows-3 distances and various fundamental plane and redshift-based distances. Error bars were omitted in this figure to avoid overcrowding, but they were of about the same size as in Figure 17.

distances, we found even stronger correlations for the 45 groups that fulfil these criteria (see Figure 15). Thereby, we reduced the impact of interlopers and imperfections of our group catalogue as well as increased the statistical quality of the distance estimate to each cluster for all methods. To be more precise, the scatter between the redshift-based distances and the Tully-Fisher relation distances is 7.5%, while the scatter between the traditional fundamental plane and the Tully-Fisher relation distances is 18.7%. Interestingly, the scatter for the corrected fundamental plane is with 17.0% only marginally lower, but it visibly reduced the systematic offset present in the traditional fundamental plane (see Figure 15). The expanded fundamental plane yields a scatter of 10.8%, when compared to the Tully-Fisher relation for the richer groups sample, and thereby also provides the best agreement between the two methods.

4.6 Comparison with CosmicFlows-3 data

The CosmicFlows (Tully et al. 2016) projects collects distances from a multitude of different methods to model the matter distribution in the local universe and the peculiar motion field. We matched the 17 669 CosmicFlows-3 galaxies to our group catalogue and excluded all galaxies in the CosmicFlows sample for which the distances were only obtained using the traditional fundamental plane (marked with *P* or *F* in their catalogue). We found 2 955 galaxies fulfilling these requirements. When comparing these distances provided by CosmicFlows-3, after rescaling to the cosmology used in our paper, to redshift-based distances for the same galaxies, we found a scatter of about 27.5% (and 24.9% for groups). We further restricted our sample in the same way as in the previous section by selecting only groups that have at least one galaxy for which we have fundamental plane distances, and one galaxy for which we have an alternative distance estimator. This left us with 339 groups (see Figure 16), that yielded correlations similar to our previous findings. The redshifts agree with a scatter of 19.7% to the CosmicFlows distances. The traditional fundamental plane exhibits the same bias as before and we obtained a scatter of 36.9%, when comparing it to the CosmicFlows distances, again due to the same systematics already discussed with the Tully-Fisher relation distances. After correcting for the dominant systematics in the residuals of the fundamental plane, we got a scatter of 31.7% between the corrected fundamental plane distances and

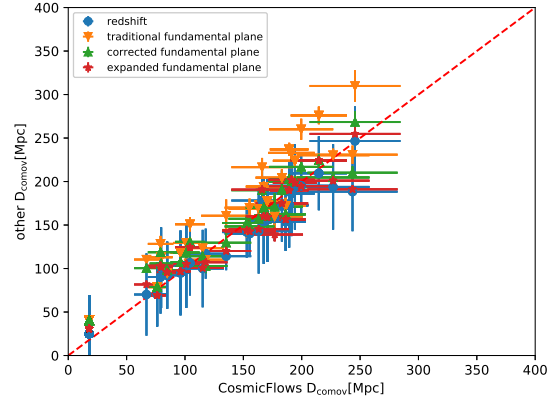


Figure 17. Comparison between CosmicFlows-3 distances and various fundamental plane and redshift-based distances for groups that host at least three galaxies with fundamental plane distances and at least three galaxies with complementary distance measurements.

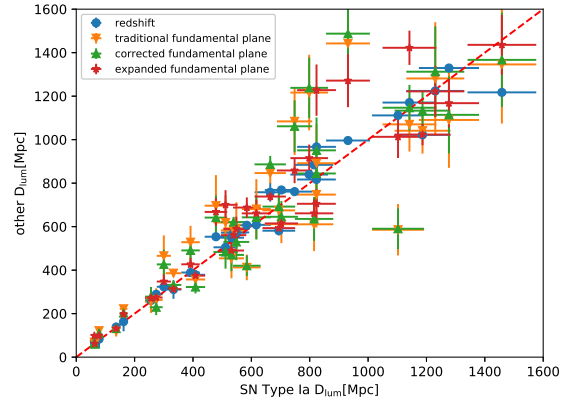


Figure 18. Comparison between Supernova Type Ia distance and various fundamental plane and redshift-based distances.

the CosmicFlows distances. Expanded fundamental plane yields a scatter of 23.5% when compared to the CosmicFlows distances.

We refined our sample by restricting it to rich groups that have at least three galaxies for which we have obtained fundamental plane distances and also at least three galaxies for which we have alternative distance measurements from CosmicFlows-3. Thereby, we found 29 groups. The scatter between the redshift-based distances and the CosmicFlows distances was found to be 12.7% for this subsample. The traditional fundamental plane clearly (see Figure 17) exhibits the same systematic offset as in the case of the Tully-Fisher distances and yields a scatter of 27.3% compared to the CosmicFlows distances. Again the corrected fundamental plane produces a slightly lower scatter of 26.7% and the expanded fundamental plane a notably lower scatter of 18.8%.

4.7 Comparison with Supernova Type Ia data

We took the catalogue of Supernova Type Ia distances⁷ from [Betoule et al. \(2014\)](#) and cross-matched it with our catalogue of various fundamental plane distances. We found that 33 of our early-type galaxies hosted Supernovae Type Ia from that catalogue. Again the traditional fundamental plane performs poorly in comparison to the Supernova Type Ia distance and we found a scatter of 27.8% (see Figure 18). The corrected fundamental plane distances have a scatter of 25.0%, when compared to the Supernova Type Ia distances. The expanded fundamental plane yields with a scatter of 21.0% compared to the Supernova Type Ia distances.

5 DISCUSSION

It can be difficult to tell, which is the optimal way to implement the fundamental plane as distance indicator. Several issues arise from the fact the SDSS spectroscopic sample is a mostly magnitude-limited, but not completely due to some colour-selected subsamples, as well as suffering from a saturation bias. Hidden and explicit redshift-dependences are problems, when one intends to use the fundamental plane as a redshift-independent distance indicator. By examining the advantages and disadvantages of the various fundamental plane calibrations and definitions, which we provided in the previous section, we want to illustrate which calibration is best-suited for which application.

5.1 Sample selection and basic methods

One of the main goals of this paper is to maximize the sample size of galaxies with fundamental plane galaxies. To this end, we had to move beyond our previous selection criteria ([Saulder et al. 2013, 2015](#)), which were dominated by the limitations of GalaxyZoo ([Lintott et al. 2008, 2011](#)). The citizen science project GalaxyZoo only provided visual morphological classifications for the galaxies covered by SDSS DR7 ([Abazajian et al. 2009](#)). Alternative approaches providing morphological classifications using machine-learning ([Domínguez Sánchez et al. 2018](#)) were also limited by their restricted sample selection (again SDSS DR7). While there are advantages in the more clearly defined such as SDSS DR7, it excludes valuable galaxies even many at the lower redshift range. As illustrated in Figure 4, we used a composite SDSS/BOSS sample based on its latest data release ([Aguado et al. 2018](#)). Our selection criteria (see Appendix A2) did not restrict our sample to any specific subset of SDSS/BOSS. Which means that if there is sufficient quality data for a galaxy in SDSS, it was used in our sample. If we had restricted ourselves to SDSS DR7, we would have missed out on 72 262 galaxies, which is a significant fraction of our dataset. The size of our sample beyond SDSS DR7 was also the reason, why we only used the data from [Simard et al. \(2011\)](#) and [Mendel et al. \(2014\)](#) only for additional tests and we could not take advantage of the data of [Meert et al. \(2015\)](#) and [Meert et al. \(2016\)](#). Our quality selection criteria ensured that our sample became increasingly sparse at higher redshifts and thereby avoiding problematic galaxies and uncertain parameter estimates. We barely had any CMASS galaxies in our sample of early-type galaxies and thereby avoided most of the problems described in [Bernardi et al. \(2011\)](#) and [Montero-Dorta et al. \(2016\)](#).

⁷ They were derived from the distance moduli listed in the cited catalogue following the procedure explained in their paper.

We used the de Vaucouleurs magnitudes and sizes from SDSS, because we found in [Saulder et al. \(2013\)](#) that they yield the best fitting values for the fundamental plane. The composite model and Petrosian magnitudes and sizes performed worse and in the Appendix of [Saulder et al. \(2015\)](#), we also showed weaker fits for the Sersic models of [Simard et al. \(2011\)](#). In contrast to this, [Bernardi et al. \(2017a\)](#) and [Bernardi et al. \(2017b\)](#) found notable deficiencies in the profile fits provided by SDSS, especially at their outer edges. However the alternative catalogues provided by them are limited to the SDSS DR7 spectroscopic sample, which cause the same problems as the other catalogues mentioned earlier. We also tested various stellar mass models provided by the SDSS database. We found that stellar masses of the Wisconsin method ([Chen et al. 2012](#)) using Maraston models ([Maraston & Strömbäck 2011](#)) works best for the expanded fundamental plane calibrations. Alternatively, we used the passive part of the stellar mass models of [Maraston et al. \(2009\)](#), which yielded a expanded fundamental plane with a larger scatter than the one provided in Section 4.4. With the stellar masses of [Maraston et al. \(2009\)](#), we found some very interesting relations for an alternative distance calibration briefly explained in Appendix C. This relation was tentative at best and did not reappear with the stellar masses of the Wisconsin method.

5.2 Traditional fundamental plane

The traditional fundamental plane has been used for about three decades and during this time various approaches, on how to calibrate it and apply it, have been developed. Since in this paper, we primarily view the fundamental plane as a distance indicator, we restrict ourselves to direct fits, which according to the very detailed work of [Sheth & Bernardi \(2012\)](#), yield the most-suitable coefficients for our applications. The selection effects due to the survey design were another issue. The common way to address it is to derive unbiased fundamental plane coefficients using volume-weights. However, given the combination of colour cuts and magnitude limits make this approach unfeasible. Hence, as illustrated in Figure 5, our sample is clearly biased. Our sample contains a disproportionately large number of bright galaxies. Since the traditional fundamental plane residuals have a strong dependence on the stellar mass, and thereby the luminosity, we would underestimate distances for bright (and thereby on average further away) galaxies. Hence, we did not use such bias corrections for our calibrations, because we wanted to gain the best-suited coefficients for our biased galaxy sample that yields the smallest error in terms of distance measurement for said sample.

One of our goals for this paper is to provide the largest possible sample of fundamental plane distances that one can obtain from the latest data release of SDSS. To this end, we slightly relaxed the selection criteria for what qualifies as an early-type galaxy in some aspects (but also tightened them up in other aspects) compared to previous work ([Saulder et al. 2013, 2015, 2016](#)). The most notable difference was dropping the GalaxyZoo ([Lintott et al. 2008](#)) classifications in favour of a more reproducible method using colours and profile fits. Thereby, we were also able to move beyond SDSS DR7 ([Abazajian et al. 2009](#)), the basis of GalaxyZoo, and include significantly more galaxies than in previous calibrations ([Saulder et al. 2013, 2015](#)). We could identify 334 388 early-type galaxies with our method and while calibrating the fundamental plane, we excluded notable outliers, mildly reducing our sample to 317 285 for which we were able to derive fundamental plane distances. [D’Onofrio et al. \(2008\)](#); [Nigoche-Netro et al. \(2009\)](#) have already shown that fundamental plane varies for different luminosity and velocity dispersion

distance indicator	$\overline{D_{\text{err,ind}}}$	$\overline{D_{\text{err,group}}}$	$\overline{D_{\text{err,sys}}}$	range $D_{\text{err,sys}}$	$\Delta_{\text{TF,all}}$	$\Delta_{\text{TF,rich}}$	$\Delta_{\text{CF3,all}}$	$\Delta_{\text{CF3,rich}}$	$\Delta_{\text{SN Ia}}$
traditional FP	20.2%	18.4%	0.3%	$\sim 0.3\%$	41.7%	18.7%	36.9%	27.3%	27.8%
corrected FP	15.9%	14.5%	0.2%	$\sim 0.2\%$	37.0%	17.0%	31.7%	26.7%	25.0%
expanded FP	9.6%	9.0%	1.1%	2.0 - 0.1 %	31.3%	10.8%	23.5%	18.8%	21.0%
redshifts	-	-	-	-	29.4%	7.5%	19.7%	12.7%	8.2%

Table 3. Summary of the different methods to obtain fundamental plane distances presented in this paper as well as redshift-based distances for comparison. First column: name of the method; second column: overall average error in the distance estimate for individual galaxies; third column: overall average error in the distance estimate for galaxy groups; fourth column: average systematic redshift-dependent error of the distance estimate; fifth column: range of the systematic redshift-dependent error of the distance estimate due to redshift-space distortions; sixth column: scatter between the respective distance indicator and the Tully-Fisher relation distances using the complete overlapping sample; seventh column: scatter between the respective distance indicator and the Tully-Fisher relation distances using only rich clusters in the overlapping sample; eighth column: scatter between the respective distance indicator and the CosmicFlows-3 distances using the complete overlapping sample; ninth column: scatter between the respective distance indicator and the CosmicFlows-3 distances using only rich clusters in the overlapping sample; tenth column: scatter between the respective distance indicator and Supernova Type-Ia distances.

ranges. When varying our selection criteria slightly for the luminosity (absolute magnitude) and central velocity dispersion ranges, we found that galaxies with very low central velocity dispersions have the most impact on the quality of our calibrations. However, a cut in this parameter also affects the sample size, which we want to keep as large as reasonably possible. Therefore, we compromise for an uncorrected velocity dispersion limit of 100 km/s, which was previously used in [Saulder et al. \(2015\)](#), and this only reduced the sample size by about 10 000 galaxies, while decreasing the distance uncertainty by 0.4 percentage points. This was a reasonable trade-off in our opinion.

An additional improvement of the fundamental plane calibrations was achieved by our group catalogue. It allowed us to correct for the redshift space distortion caused by the peculiar motions of galaxies in clusters. This worked in two ways. First, it help with the calibration of the fundamental plane (or actually fundamental planes, since we also used the same method for the stellar mass fundamental plane), because we used the median group redshift instead of the individual redshifts of the galaxies, when we derived the fundamental plane parameters⁸. Additionally, we used it to reduce the distance uncertainties to groups that hosted more than one early-type galaxy for which we were able to derive a fundamental plane distance. By taking the median of the fundamental plane distance of the different early-type galaxies, we could improve the distance estimate to these groups and clusters significantly. Using the median instead of the mean has the advantage that it is less sensitive towards interlopers that plague all FoF-based group catalogues. The group catalogue will also help us in our future research, when we will take a quality selected subsample from our distance catalogue to study peculiar motions.

The magnitudes used for the traditional fundamental plane were corrected for evolutionary effects using Equation 15, which based on the established method by [Bernardi et al. \(2003\)](#). Assuming a constant number density of the brightest galaxies, we derived a Q parameter of 0.71 mag/ z , which is slightly lower than previous estimates ([Bernardi et al. 2003](#); [Saulder et al. 2013](#)) using different methods. We argue that adjusting the evolution effects for the brightest galaxies is sufficient for our application, because at the higher redshifts, when evolution becomes the most relevant, those galaxies are the only ones still detected within the sample. However, evolution corrections have an explicit redshift dependence, which creates a small systematic bias. Furthermore, the surface brightnesses used for the fundamental plane have to be corrected for Tolman effect,

which dims surface brightnesses as a function of the cosmological redshift (hence distance). Although the K-corrections are, by their very nature, also redshift-dependent, this is not an issue for them. The K-correction only corrects the shift in the spectral energy distribution, which depends on the observed redshift (caused by peculiar motions and the Hubble expansion). Therefore, there is no implicit pure distance dependence on this correction (it does not matter what caused the redshift). In contrast to this, the evolution correction as well as the correction for the Tolman effect depend explicitly on the cosmological redshift which correlates with the distance. However, one cannot measure the cosmological redshift directly, because in practice, the observed redshift is the sum of the cosmological redshift and the redshift caused by peculiar motions. In order to estimate the systematic effect, we introduced a Gaussian scatter of the same magnitude as the average 1-dimensional peculiar velocities of the groups (~ 340 km/s) with the help of our mock catalogues. By comparing the distances obtained from the perturbed and unperturbed data, we found a systematic bias of 0.3% on the distance estimates caused by the hidden redshift-dependences and redshift-space distortions.

We tested the dependences of the residuals of the traditional fundamental plane on several parameters. We focussed on parameters that are (mostly) independent of the parameters of the traditional fundamental plane. Using the data of [Simard et al. \(2011\)](#), we could not find any dependence on the Sersic parameter for our sample of early-type galaxies. There is a clear dependence on the number of (early-type) galaxies per group, which will be discussed in the section in more detail. Also the dependence on the stellar masses ([Maraston & Strömbäck 2011](#); [Chen et al. 2012](#)) will be discussed along with the expanded fundamental plane. Using the data from MaNGA ([Bundy et al. 2015](#)), we were able also test the dependence on the λ_R parameter, which according to ([Graham et al. 2018](#)) correlates with the stellar mass. However using the same data, we could not find any notable dependence between the λ_R parameter ([Emmellem et al. 2007](#)) and the residuals of the traditional fundamental plane. We did not find any correlation for the residuals and galaxy colours or axis-ratios.

5.3 Corrected fundamental plane

To account for the systematic biases of the traditional fundamental plane, we measured the mean residuals in bins in redshift-magnitude space. By adding a fitting function based on the residuals to the fundamental plane, we were not only able to remove the most dominant systematic bias, but also notably reduced the scatter. This correction also removed the systematic offset of nearby galaxies in rich clusters seen in Figures 15 and 17. We illustrated in Figure 19 that it the sys-

⁸ The magnitudes used to derive the surface brightnesses were evolution corrected. Also the estimated distances to get R_e for the calibration made use of the group redshifts.

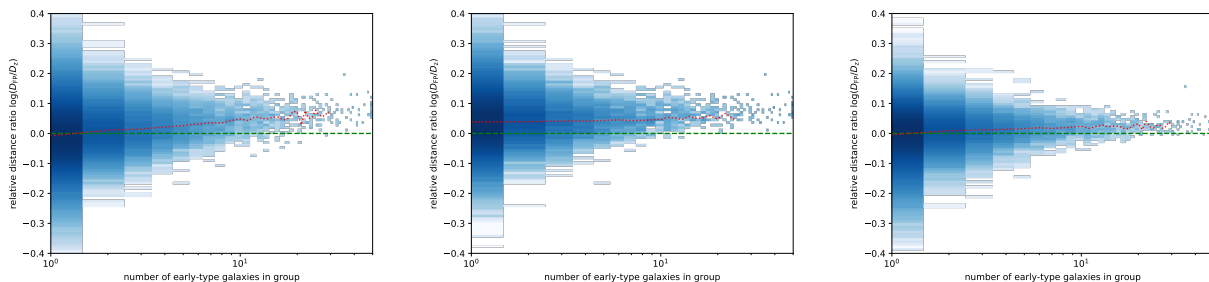


Figure 19. Dependence of the fundamental plane residuals on the number of early-type galaxies per group. Left panel: residuals of the traditional fundamental plane using the entire sample; central panel: residuals of the traditional fundamental plane only using the galaxies with a redshift of less than 0.1; right panel: residuals of the corrected fundamental plane using the entire sample.

tematic bias that correlates with the richness (in early-type) galaxies of the groups/clusters is visibly reduced. Furthermore, there is no systematic offset of the residuals of corrected fundamental plane for nearby clusters in contrast to the traditional fundamental plane.

Aside from removing notable systematics, the overall scatter of the corrected fundamental plane is reduced to 14.5%. Despite our correction function being redshift-dependent, the overall redshift-dependent systematics due to redshift-space distortions are with just 0.2% comparable to the ones from the traditional fundamental plane. The correction function, which we used is just a simple and effective model, that is best suited for our large and complex sample of early-type galaxies. There is some room for further improvement to get possibly better distances using a fully Bayesian model similar to Howlett et al. (2017) and Qin et al. (2018) to correct for systematics, but only for a smaller and well-defined subsample. However to maximize the galaxy sample, the corrected fundamental plane is the best save improvement of the systematically biased traditional fundamental plane calibrations.

5.4 Expanded fundamental plane

There is a clear (absolute) luminosity dependence of the traditional fundamental plane (see Figure 5), which naturally causes problems for magnitude-limited surveys. Also one cannot use the absolute magnitudes obtained from redshift-distances to improve the (redshift-independent) fundamental plane without being plagued by countless other systematic biases. Aside from using the corrected fundamental plane, we tried to address this in many different ways, which are briefly discussed in Appendix C. The stellar mass roughly correlates with the absolute magnitudes and it can be estimated by fitting spectro-photometric models of the spectral energy distribution using the method of Chen et al. (2012) and the models of Maraston & Strömbäck (2011) as provided by SDSS. By using their stellar masses as an additional parameter for the fundamental plane⁹, we could noticeably reduce the scatter of the distances obtained from this relation. As illustrated in Figure 11, higher quality stellar masses (Graham et al. 2018) as those derived from integral field surveys such as in this case of MaNGA (Bundy et al. 2015), have the potential to further improve the distance estimates. We also tested other stellar mass estimates provided by SDSS such the photometric stellar masses using the method of Maraston et al. (2009) and Maraston et al. (2013). We found a notably larger scatter than

using these stellar masses and the coefficients would be different. Most notably the a_{exp} coefficient is more important with the photometric stellar masses than with the spectro-photometric stellar masses. This makes sense, since the central velocity dispersion was used the calibrations using the method of Chen et al. (2012).

For our definition of the expanded fundamental plane (see Equation 23), we took advantage of the dominant bias and added a term to the traditional fundamental plane for the stellar mass dependence. This way we could remove the some of the systematic bias at low redshift while also significantly reducing the overall scatter of our distance estimates. We found a scatter of 9.6% for the distances obtained from the expanded fundamental plane, when compared to the redshift-distance used for calibration. The average systematic redshift dependent bias is with 1.1%, which is notably larger than for the traditional and corrected fundamental plane. However, there is the hidden redshift dependence in the stellar mass models used, which was difficult to exactly quantify. Therefore to test its impact on the systematics, we simply rescaled the stellar masses according to the introduced redshift perturbation introduced in the previous subsection by considering the difference in real and derived luminosity distance). Another problem is that the magnitude of the systematic bias depends on the the redshift itself and reaches higher values (up to 2%) for nearby galaxies. This will have to be taken into account, when deriving peculiar motions from these distances.

5.5 Comparison with other distance indicators

In order to test our fundamental plane distances, we compared them to both redshift-based distances and other distance indicators. Since we used them for calibrations, we have redshift-based distances to all galaxies in our sample at our disposal. Additionally, we obtained Supernovae Type Ia distance to a small subset of our galaxies. Furthermore, by using our group catalogue, we were able to determine Tully-Fisher relation distances to nearby groups hosting both early- and late-type galaxies and used them for comparison as well. Moreover, we took advantage of the CosmicFlows-3 (Tully et al. 2016) sample to test our distance estimates. The comparison with the redshift-based distances yielded an upper-limit for the statistical error of our calibration, because the redshift-based distances are biased themselves by the peculiar motions of the galaxy groups¹⁰.

¹⁰ Not individual galaxies, because we used our group catalogue to correct for the redshift-space distortions in clusters, but might get occasional additional bias from interlopers in return.

⁹ Strictly speaking it is not a plane any more, but a hyper-plane then.

Furthermore, the complementary distance indicators allowed us to test the quality of our calibrations and to better check for any systematic biases (see Table 3 for a brief overview and comparison of our results).

It is impossible to compare Tully-Fisher relation distances and fundamental plane distances directly, because by their very definition they target mutually exclusive types of galaxies. However our group catalogue allowed us to compare these two distance indicators for several galaxy groups and clusters. The slight disadvantage of this method is that group catalogues are not perfect and there might be interlopers affecting the dataset. The only ways to minimize this effect is by taking rich groups and median distances. When just merging the Tully-Fisher relation distances obtained from the NASA/IPAC Extragalactic Database with our group catalogue and comparing them to the redshift-based distances, we obtained an uncertainty of about 23.5% (23.5% without the group catalogue), which is worse than the traditional fundamental plane. Considering that the Tully-Fisher relation distances are compiled from various sources, both indicators can be considered to be of about the same overall quality. However, the traditional fundamental plane exhibits a strong systematic bias (see Figure 14) at short distances, which becomes very apparent in this test, because Tully-Fisher relation data only reaches out to about 300 Mpc. This is due to the SDSS saturation bias, which excludes the brightest galaxies from the main galaxy sample) in the nearby universe as well as due to selection effects introduced by the survey design. As illustrated in Figure 5, there is a systematic bias in the traditional fundamental plane depending on intrinsic brightness of galaxies. Therefore, the fundamental plane distances, which are calibrated for the entire range of magnitudes¹¹ of the SDSS and BOSS sample, are systematically overestimated. In contrast to this, both the corrected fundamental plane and the expanded fundamental plane are not affected by this bias, not even for rich clusters where it is the most striking for the traditional fundamental plane (see Figure 15).

We repeated the same procedure with the CosmicFlows-3 (Tully et al. 2016) dataset from which we only excluded all fundamental plane distances. The advantage of the CosmicFlows-3 sample compared to the Tully-Fisher relation distances obtained from NED are that it is consistently calibrated. As illustrated in Figures 16 and 17, the overall behaviour is fairly similar to the Tully-Fisher relation distances sample. Due to the overlap between the two samples, this is expected.

Supernovae Type Ia are rare, but out of the 740 supernovae in the database of Betoule et al. (2014), we found 33 within our sample of galaxies with fundamental plane distances. The main advantage of the supernovae Type Ia dataset is that they cover a much wider range in distances than the Tully-Fisher relation dataset. The supernovae Type Ia dataset does not show any notable systematic biases (see Figure 18) for any fundamental plane. Furthermore, there is a minor discrepancy between the redshifts from the supernova catalogue and the SDSS redshifts, but using the other redshifts from the supernova catalogue instead only marginally decreases the error between the supernovae distances and the redshifts to 7%¹², while slightly increasing all other errors.

¹¹ We double-check that this is not due to the lack of a Malmquist-bias/saturation correction by also looking at the distances derived using the fundamental plane coefficients obtained using volume-weights. We found a similar (actually slightly worse) systematically biased distribution.

¹² And would remain at 8%, if taking all 740 galaxies of the supernova catalogue.

6 SUMMARY AND CONCLUSIONS

We used the latest data release from SDSS (Aguado et al. 2018) to derive the largest set of fundamental plane distances to date. We provided a comprehensive catalogue of fundamental plane distances to 317 285 galaxies up to a redshift of 0.4. We calculated distances using the traditional fundamental plane, as well as two alternative variants of the fundamental plane, which we called the corrected fundamental plane and the expanded fundamental plane. Additionally, we constructed a FoF group catalogue based on the SDSS spectroscopic sample up to a redshift of 0.5, which was supplemented by 2MRS (Huchra et al. 2012) data to partially compensate for the saturation limit of SDSS spectroscopy. This group catalogue helped us to reduce the scatter of distances obtained from the traditional fundamental plane from an average of 20.2% down to an average of 18.4%. Additionally, it allowed us to conduct further tests of our distance calibrations by helping us to compare our fundamental plane distances to Tully-Fisher relation distances obtained from NED, distances from the CosmicFlows-3 (Tully et al. 2016) sample, and supernovae Type Ia distance obtained from (Betoule et al. 2014).

We defined the corrected fundamental plane to combat systematic biases affecting the traditional fundamental plane by adding a correction function that removes said biases. Although this function is explicitly redshift dependent, we did not measure any increase in the systematics due to redshift-space distortions. With a reduced scatter of the distance estimates to 14.5%, we consider best and safest way to improve the traditional fundamental plane. A more experimental way to even further reduce the uncertainties in the distance measurements is the expanded mass fundamental plane, which we obtained by adding a term proportional to the stellar mass to the definition of the traditional fundamental plane. While we were able to reduce the scatter of the distance measurements using the expanded fundamental plane to only 9.0%, which is half the value of the traditional fundamental plane, we found it to be strongly dependent on the specific stellar mass model. Furthermore, the cross-correlations between the stellar masses and various parameters created additional problems with the systematics from redshift-space distortions. While the improvements in the overall scatter are great for the expanded fundamental plane, the increased systematics will cause problems for future peculiar motion studies using these distances. We consider the corrected fundamental plane as the best approach of obtaining redshift-independent distances using our methods.

A detailed description of our complete set of catalogues can be found in Appendix B. In the future we hope to use quality selected subsets of our catalogues using some of the improved fundamental plane distances for peculiar velocity studies and to further our understanding of the matter distribution in the local universe.

ACKNOWLEDGMENTS

We want to thank David Parkison, Benjamin Joachimi, and Shraavan Shetty for inspiring discussions. We also acknowledge helpful advise from Suhail Dhawan and Barry F. Madore. Furthermore, we want to thank Maret Einasto and Cullan Howlett for some important comments and suggestions.

Funding for the Sloan Digital Sky Survey IV has been provided by the Alfred P. Sloan Foundation, the U.S. Department of Energy Office of Science, and the Participating Institutions. SDSS-IV acknowledges support and resources from the Center for High-

Performance Computing at the University of Utah. The SDSS web site is www.sdss.org.

SDSS-IV is managed by the Astrophysical Research Consortium for the Participating Institutions of the SDSS Collaboration including the Brazilian Participation Group, the Carnegie Institution for Science, Carnegie Mellon University, the Chilean Participation Group, the French Participation Group, Harvard-Smithsonian Center for Astrophysics, Instituto de Astrofísica de Canarias, The Johns Hopkins University, Kavli Institute for the Physics and Mathematics of the Universe (IPMU) / University of Tokyo, Lawrence Berkeley National Laboratory, Leibniz Institut für Astrophysik Potsdam (AIP), Max-Planck-Institut für Astronomie (MPIA Heidelberg), Max-Planck-Institut für Astrophysik (MPA Garching), Max-Planck-Institut für Extraterrestrische Physik (MPE), National Astronomical Observatories of China, New Mexico State University, New York University, University of Notre Dame, Observatório Nacional / MCTI, The Ohio State University, Pennsylvania State University, Shanghai Astronomical Observatory, United Kingdom Participation Group, Universidad Nacional Autónoma de México, University of Arizona, University of Colorado Boulder, University of Oxford, University of Portsmouth, University of Utah, University of Virginia, University of Washington, University of Wisconsin, Vanderbilt University, and Yale University.

This publication makes use of data products from the Two Micron All Sky Survey, which is a joint project of the University of Massachusetts and the Infrared Processing and Analysis Center/California Institute of Technology, funded by the National Aeronautics and Space Administration and the National Science Foundation.

We thank the Korea Institute for Advanced Study for providing computing resources (KIAS Center for Advanced Computation Linux Cluster System) for this work.

This research has made use of the NASA/IPAC Extragalactic Database (NED) which is operated by the Jet Propulsion Laboratory, California Institute of Technology, under contract with the National Aeronautics and Space Administration.

The codes required for this project were written in PYTHON. We want to take the opportunity to thank all its developers and especially the people behind the following packages: SCIPY (Jones et al. 01), NUMPY (van der Walt et al. 2011), MATPLOTLIB (Barrett et al. 2005), and ASTROPY (Astropy Collaboration et al. 2013; Price-Whelan et al. 2018), who get far too little recognition and too few citations despite their work being regularly used by a large fraction of the astronomical community.

REFERENCES

- Abazajian K. N., et al., 2009, *ApJS*, **182**, 543
 Aguado D. S., et al., 2018, arXiv e-prints, p. [arXiv:1812.02759](https://arxiv.org/abs/1812.02759)
 Ahn C. P., et al., 2012, *ApJS*, **203**, 21
 Astropy Collaboration et al., 2013, *A&A*, **558**, A33
 Bacon R., et al., 2001, *MNRAS*, **326**, 23
 Barrett P., Hunter J., Miller J. T., Hsu J.-C., Greenfield P., 2005, in Shopbell P., Britton M., Ebert R., eds, *Astronomical Society of the Pacific Conference Series Vol. 347, Astronomical Data Analysis Software and Systems XIV*. p. 91
 Beers T. C., Flynn K., Gebhardt K., 1990, *AJ*, **100**, 32
 Beifiori A., et al., 2014, *ApJ*, **789**, 92
 Beifiori A., et al., 2015, IAU General Assembly, **22**, 2243875
 Beifiori A., et al., 2017, *ApJ*, **846**, 120
 Bernardi M., et al., 2003, *AJ*, **125**, 1866
 Bernardi M., Roche N., Shankar F., Sheth R. K., 2011, *MNRAS*, **412**, L6
 Bernardi M., Meert A., Sheth R. K., Fischer J. L., Huertas-Company M., Maraston C., Shankar F., Vikram V., 2017a, *MNRAS*, **467**, 2217
 Bernardi M., Fischer J. L., Sheth R. K., Meert A., Huertas-Company M., Shankar F., Vikram V., 2017b, *MNRAS*, **468**, 2569
 Betoule M., et al., 2014, *A&A*, **568**, A22
 Bezanson R., van Dokkum P. G., van de Sande J., Franx M., Leja J., Kriek M., 2013, *ApJ*, **779**, L21
 Bilir S., Ak S., Karaali S., Cabrera-Lavers A., Chonis T. S., Gaskell C. M., 2008, *MNRAS*, **384**, 1178
 Bolton A. S., Treu T., Koopmans L. V. E., Gavazzi R., Moustakas L. A., Burles S., Schlegel D. J., Wayth R., 2008, *ApJ*, **684**, 248
 Bundy K., et al., 2015, *ApJ*, **798**, 7
 Busarello G., Capaccioli M., Capozziello S., Longo G., Puddu E., 1997, *A&A*, **320**, 415
 Busarello G., Lanzoni B., Capaccioli M., Longo G., Colless M. M., Graham A. W., 1998, *Mem. Soc. Astron. Italiana*, **69**, 217
 Campbell L. A., et al., 2014, *MNRAS*, **443**, 1231
 Cappellari M., et al., 2006, *MNRAS*, **366**, 1126
 Cappellari M., et al., 2007, *MNRAS*, **379**, 418
 Cappellari M., et al., 2011, *MNRAS*, **413**, 813
 Cappellari M., et al., 2013, *MNRAS*, **432**, 1709
 Chen Y.-M., et al., 2012, *MNRAS*, **421**, 314
 Chilingarian I. V., Melchior A., Zolotukhin I. Y., 2010, *MNRAS*, **405**, 1409
 Chiu M.-C., Ko C.-M., Shu C., 2017, *Phys. Rev. D*, **95**, 063020
 Ciotti L., Lanzoni B., Renzini A., 1996, *MNRAS*, **282**, 1
 Colless M., Saglia R. P., Burstein D., Davies R. L., McMahan R. K., Wegner G., 2001, *MNRAS*, **321**, 277
 Croom S. M., et al., 2012, *MNRAS*, **421**, 872
 D’Onofrio M., Valentinuzzi T., Secco L., Caimmi R., Bindoni D., 2006, *New Astron. Rev.*, **50**, 447
 D’Onofrio M., et al., 2008, *ApJ*, **685**, 875
 D’Onofrio M., et al., 2013, *MNRAS*, **435**, 45
 D’Onofrio M., Cariddi S., Chiosi C., Chiosi E., Marziani P., 2017, *ApJ*, **838**, 163
 Dawson K. S., et al., 2013, *AJ*, **145**, 10
 Desmond H., Wechsler R. H., 2017, *MNRAS*, **465**, 820
 Djorgovski S., Davis M., 1987, *ApJ*, **313**, 59
 Domínguez Sánchez H., Huertas-Company M., Bernardi M., Tuccillo D., Fischer J. L., 2018, *MNRAS*, **476**, 3661
 Dressler A., Lynden-Bell D., Burstein D., Davies R. L., Faber S. M., Terlevich R., Wegner G., 1987, *ApJ*, **313**, 42
 Duarte M., Mamon G. A., 2014, *MNRAS*, **440**, 1763
 Eke V. R., et al., 2004, *MNRAS*, **348**, 866
 Emsellem E., et al., 2007, *MNRAS*, **379**, 401
 Emsellem E., et al., 2011, *MNRAS*, **414**, 888
 Faber S. M., Jackson R. E., 1976, *ApJ*, **204**, 668
 Fraix-Burnet D., Dugué M., Chattopadhyay T., Chattopadhyay A. K., Davoust E., 2010, *MNRAS*, **407**, 2207
 Gallazzi A., Charlot S., Brinchmann J., White S. D. M., 2006, *MNRAS*, **370**, 1106
 Gargiulo A., et al., 2009, *MNRAS*, **397**, 75
 Gibbons R. A., Fruchter A. S., Bothun G. D., 2001, *AJ*, **121**, 649
 Graham A., Colless M., 1997, *MNRAS*, **287**, 221
 Graham M. T., et al., 2018, *MNRAS*, **477**, 4711
 Guo Q., et al., 2011, *MNRAS*, **413**, 101
 Guo Q., White S., Angulo R. E., Henriques B., Lemson G., Boylan-Kolchin M., Thomas P., Short C., 2013, *MNRAS*, **428**, 1351
 Guzman R., Lucey J. R., Bower R. G., 1993, *MNRAS*, **265**, 731

- Hou L., Wang Y., 2015, *Research in Astronomy and Astrophysics*, **15**, 651
- Howlett C., et al., 2017, *MNRAS*, **471**, 3135
- Hubble E., Tolman R. C., 1935, *ApJ*, **82**, 302
- Huchra J. P., et al., 2012, *ApJS*, **199**, 26
- Hudson M. J., Lucey J. R., Smith R. J., Steel J., 1997, *MNRAS*, **291**, 488
- Hyde J. B., Bernardi M., 2009a, *MNRAS*, **394**, 1978
- Hyde J. B., Bernardi M., 2009b, *MNRAS*, **396**, 1171
- Joachimi B., Singh S., Mandelbaum R., 2015, *MNRAS*, **454**, 478
- Jones E., Oliphant T., Peterson P., et al., 2001–, SciPy: Open source scientific tools for Python, <http://www.scipy.org/>
- Jørgensen I., Franx M., Kjaergaard P., 1993, in I. J. Danziger, W. W. Zeilinger, & K. Kjær ed., *European Southern Observatory Conference and Workshop Proceedings Vol. 45*, European Southern Observatory Conference and Workshop Proceedings. pp 71–+
- Jørgensen I., Franx M., Kjaergaard P., 1995, *MNRAS*, **276**, 1341
- Jørgensen I., Franx M., Kjaergaard P., 1996, *MNRAS*, **280**, 167
- Jørgensen I., Chiboucas K., Flint K., Bergmann M., Barr J., Davies R., 2006, *ApJ*, **639**, L9
- Jovanović V. B., Capozziello S., Jovanović P., Borka D., 2016, *Physics of the Dark Universe*, **14**, 73
- Kelson D. D., Illingworth G. D., van Dokkum P. G., Franx M., 2000, *ApJ*, **531**, 184
- Kipper R., Tamm A., Tenjes P., Tempel E., 2016, in van de Weygaert R., Shandarin S., Saar E., Einasto J., eds, *IAU Symposium Vol. 308, The Zeldovich Universe: Genesis and Growth of the Cosmic Web*. pp 471–472, doi:10.1017/S1743921316010401
- Komatsu E., et al., 2011, *ApJS*, **192**, 18
- Kormendy J., 1977, *ApJ*, **218**, 333
- La Barbera F., Busarello G., Merluzzi P., de la Rosa I. G., Coppola G., Haines C. P., 2008, *ApJ*, **689**, 913
- La Barbera F., de Carvalho R. R., de La Rosa I. G., Lopes P. A. A., 2010a, *MNRAS*, **408**, 1335
- La Barbera F., Lopes P. A. A., de Carvalho R. R., de La Rosa I. G., Berlind A. A., 2010b, *MNRAS*, **408**, 1361
- Lintott C. J., et al., 2008, *MNRAS*, **389**, 1179
- Lintott C., et al., 2011, *MNRAS*, **410**, 166
- Lucey J. R., Bower R. G., Ellis R. S., 1991, *MNRAS*, **249**, 755
- Magoulas C., et al., 2012, *MNRAS*, **427**, 245
- Magoulas C., et al., 2013, in Thomas D., Pasquali A., Ferreras I., eds, *IAU Symposium Vol. 295, The Intriguing Life of Massive Galaxies*. pp 233–233, doi:10.1017/S1743921313004882
- Maraston C., Strömbäck G., 2011, *MNRAS*, **418**, 2785
- Maraston C., Strömbäck G., Thomas D., Wake D. A., Nichol R. C., 2009, *MNRAS*, **394**, L107
- Maraston C., et al., 2013, *MNRAS*, **435**, 2764
- Meert A., Vikram V., Bernardi M., 2015, *MNRAS*, **446**, 3943
- Meert A., Vikram V., Bernardi M., 2016, *MNRAS*, **455**, 2440
- Mendel J. T., Simard L., Palmer M., Ellison S. L., Patton D. R., 2014, *ApJS*, **210**, 3
- Montero-Dorta A. D., Shu Y., Bolton A. S., Brownstein J. R., Weiner B. J., 2016, *MNRAS*, **456**, 3265
- Müller K. R., Freudling W., Watkins R., Wegner G., 1998, *ApJ*, **507**, L105
- Mutabazi T., Blyth S. L., Woudt P. A., Lucey J. R., Jarrett T. H., Bilicki M., Schröder A. C., Moore S. A. W., 2014, *MNRAS*, **439**, 3666
- Nigoche-Netro A., Ruelas-Mayorga A., Franco-Balderas A., 2009, *MNRAS*, **392**, 1060
- Oldham L., Auger M., Fassnacht C. D., Treu T., Koopmans L. V. E., Lagattuta D., McKean J., Vegetti S., 2017, *MNRAS*, **470**, 3497
- Padmanabhan N., et al., 2004, *New Astron.*, **9**, 329
- Pahre M. A., Djorgovski S. G., de Carvalho R. R., 1996, *ApJ*, **456**, L79
- Pahre M. A., de Carvalho R. R., Djorgovski S. G., 1998, *AJ*, **116**, 1606
- Planck Collaboration et al., 2015, preprint, (arXiv:1502.01589)
- Price-Whelan A. M., et al., 2018, *AJ*, **156**, 123
- Qin F., Howlett C., Staveley-Smith L., Hong T., 2018, *MNRAS*, **477**, 5150
- Robotham A. S. G., et al., 2011, *MNRAS*, **416**, 2640
- Rykoff E. S., et al., 2014, *ApJ*, **785**, 104
- Samir R. M., Reda F. M., Shaker A. A., Osman A. M. I., Amin M. Y., 2016, *NRIAG Journal of Astronomy and Geophysics*, **5**, 277
- Sandage A., Perelmuter J.-M., 1990a, *ApJ*, **350**, 481
- Sandage A., Perelmuter J.-M., 1990b, *ApJ*, **361**, 1
- Sandage A., Perelmuter J.-M., 1991, *ApJ*, **370**, 455
- Saulder C., Mieske S., Zeilinger W. W., Chilingarian I., 2013, *A&A*, **557**, A21
- Saulder C., van den Bosch R. C. E., Mieske S., 2015, *A&A*, **578**, A134
- Saulder C., van Kampen E., Chilingarian I. V., Mieske S., Zeilinger W. W., 2016, *A&A*, **596**, A14
- Schechter P. L., 1980, *AJ*, **85**, 801
- Schechter P. L., 2016, in Bragaglia A., Arnaboldi M., Rejkuba M., Romano D., eds, *IAU Symposium Vol. 317, The General Assembly of Galaxy Halos: Structure, Origin and Evolution*. pp 35–38, doi:10.1017/S1743921315007267
- Schechter P. L., Pooley D., Blackburne J. A., Wambsganss J., 2014, *ApJ*, **793**, 96
- Schlegel D. J., Finkbeiner D. P., Davis M., 1998, *ApJ*, **500**, 525
- Scodreggio M., Gavazzi G., Belsole E., Pierini D., Boselli A., 1998, *MNRAS*, **301**, 1001
- Scott N., et al., 2015, *MNRAS*, **451**, 2723
- Sheth R. K., Bernardi M., 2012, *MNRAS*, **422**, 1825
- Simard L., Mendel J. T., Patton D. R., Ellison S. L., McConnachie A. W., 2011, *ApJS*, **196**, 11
- Skrutskie M. F., et al., 2006, *AJ*, **131**, 1163
- Smith R. J., Lucey J. R., Schlegel D. J., Hudson M. J., Baggle G., Davies R. L., 2001, *MNRAS*, **327**, 249
- Smith R. J., et al., 2004, *AJ*, **128**, 1558
- Springel V., et al., 2005, *Nature*, **435**, 629
- Springob C. M., et al., 2012, *MNRAS*, **420**, 2773
- Suzuki N., et al., 2012, *ApJ*, **746**, 85
- Taranu D., Dubinski J., Yee H. K. C., 2015, *ApJ*, **803**, 78
- Terlevich R., Davies R. L., Faber S. M., Burstein D., 1981, *MNRAS*, **196**, 381
- Tolman R. C., 1930, *Proceedings of the National Academy of Science*, **16**, 511
- Tonry J. L., Davis M., 1981, *ApJ*, **246**, 680
- Trujillo I., Burkert A., Bell E. F., 2004, *ApJ*, **600**, L39
- Tully R. B., Fisher J. R., 1977, *A&A*, **54**, 661
- Tully R. B., Courtois H. M., Sorce J. G., 2016, *AJ*, **152**, 50
- Wegner G., Colless M., Saglia R. P., McMahan R. K., Davies R. L., Burstein D., Baggle G., 1999, *MNRAS*, **305**, 259
- Willmer C. N. A., 2018, *The Astrophysical Journal Supplement Series*, **236**, 47
- Yang X., Mo H. J., van den Bosch F. C., Pasquali A., Li C., Barden M., 2007, *ApJ*, **671**, 153
- Zahid H. J., Damjanov I., Geller M. J., Chilingarian I., 2015, *ApJ*, **806**, 122

Zahid H. J., Damjanov I., Geller M. J., Hwang H. S., Fabricant D. G., 2016, *ApJ*, **821**, 101
 de Carvalho R. R., Djorgovski S., 1992, *ApJ*, **389**, L49
 van de Sande J., Kriek M., Franx M., Bezanson R., van Dokkum P. G., 2014, *ApJ*, **793**, L31
 van de Sande J., et al., 2017, *MNRAS*, **472**, 1272
 van der Walt S., Colbert S. C., Varoquaux G., 2011, *Computing in Science and Engineering*, **13**, 22

APPENDIX A: DETAILED SELECTION CRITERIA

A1 Group data selection

We selected galaxies in SDSS DR15 (Aguado et al. 2018) using the following set of criteria:

- covered by SDSS/BOSS spectroscopy (*SpecObj.bestobjID* ≠ 0)
- photometrically identified as a galaxy (*PhotoObj.type* = 3)
- spectroscopically identified as a galaxy or QSO (*SpecObj.class* = 'GALAXY' OR *SpecObj.class* = 'QSO')
- redshift between zero and 0.51 (*SpecObj.z* < 0.51 AND *SpecObj.z* > 0)
- clean spectroscopic data (*SpecObj.zWarning* = 0)
- no data from known problematic BOSS plates (*((SpecObj.tile* ≥ 10324) AND (*SpecObj.instrument* = 'BOSS'))
- OR (*SpecObj.instrument* = 'SDSS'))).

For all galaxies selected using these criteria, we obtained the following parameters from SDSS:

- photometric object ID (*PhotoObj.objID*)
- galactic coordinates (*PhotoObj.b* and *PhotoObj.l*)
- spectroscopic redshifts (*SpecObj.z*)
- composite model magnitudes in the g,r,i, and z band (*PhotoObj.cModelMag_X*¹³) and the corresponding error (*PhotoObj.petroMagErr_X*)
- the galactic extinction values associated with these galaxies (*PhotoObj.extinction_X*) based on Schlegel maps (Schlegel et al. 1998).

A2 Early-type galaxy selection

We required our sample of early-type galaxies to fulfil the following set of criteria:

- redshift lower than 0.5 (*SpecObj.z* < 0.5)
- spectroscopically identified to be a galaxy¹⁴ (*SpecObj.class* = 'GALAXY')
- central velocity dispersion between 60 and 420 km/s (*SpecObj.veldisp* > 60 AND *SpecObj.veldisp* < 420)
- decent spectroscopic signal-to-noise ratios (*SpecObj.snMedian* > 10)
- no edge-on or strongly inclined S0-galaxies (defined by an axis-ratio greater than 0.7) in any¹⁵ band (*PhotoObj.deVAB_X* < 0.7)

¹³ To condense our notation a little, we used the wildcard X to indicate that we obtained this quantity for the g, r, i, and z band.

¹⁴ QSOs are not longer allowed, when compared to the sample used for the group catalogue.

¹⁵ We are referring to the main SDSS bands minus the problematic u band only. Therefore, by 'any band' or 'every band', we always refer to the SDSS g, r, i, and z-bands.

- likelihood for a de Vaucouleurs-profile has to be greater than for an exponential profile in every band (*PhotoObj.lnLDeV_X* > *PhotoObj.lnLEXP_X*)
- de Vaucouleurs-profiles have high fitting fractions in every band (*PhotoObj.fracDeV_X* > 0.8)
- object is increasingly brighter in redder bands (*PhotoObj.deVMag_g* > *PhotoObj.deVMag_r* > *PhotoObj.deVMag_i* > *PhotoObj.deVMag_z*)
- extinction corrected g-r is greater than 0.65 mag (*((P.deVMag_g - P.extinction_g) - (P.deVMag_r - P.extinction_r))* > 0.65)
- extinction corrected g-z is greater than 1 mag (*((P.deVMag_g - P.extinction_g) - (P.deVMag_z - P.extinction_z))* > 1.0).

For the selected objects, we downloaded the following parameters:

- photometric object ID (*PhotoObj.objID*),
- DR7 photometric object ID (if available¹⁶) for cross-matching with value-added catalogues (*PhotoObjDR7.dr7objid*)
- equatorial coordinates (*PhotoObj.ra* and *PhotoObj.dec*)
- galactic coordinates (*PhotoObj.b* and *PhotoObj.l*)
- spectroscopic redshifts (*SpecObj.z*)
- central velocity dispersions (*SpecObj.veldisp*)
- identifier of the spectroscopic instrument¹⁷ (*SpecObj.instrument*)
- semi-major/minor axis ratio in every band (*PhotoObj.deVAB_X*)
- de Vaucouleur radii in every band (*PhotoObj.deVRad_X*)
- de Vaucouleur model magnitudes in every band (*PhotoObj.deVMag_X*)
- galactic extinction values associated with the coordinates of these galaxies (*PhotoObj.extinction_X*)
- stellar masses (if available) (*stellarMassPCAW-iscM11.mstellar_median*) according to Wisconsin method (Chen et al. 2012) using Maraston models (Maraston & Strömbäck 2011).

A3 Selection of galaxies for fundamental plane calibrations

We further filtered the early-type galaxies selected according to Appendix A2 to obtain the sample, which we used for our fundamental plane calibration, by applying the following selection criteria:

- evolution corrected absolute magnitudes M_{abs} between -25.5 mag and -19 mag in the z band
- g-r colour between 2.5 mag and -1.5 mag
- radius of log(R_e/kpc) between -0.5 dex and 1.5 dex in any filter
- uncorrected velocity dispersion greater than 100 km/s
- redshifts less than 0.4 (in the CMB-rest frame)

Additionally, we used the sample after this first cleansing to determine the red sequence in the colour-magnitude diagram¹⁸. We removed:

- 5- σ outliers from the first iteration of the traditional fundamental plane in any filter
- g-z colour bluer than 1 mag
- 3- σ outliers from the red sequence.

¹⁶ a LEFT (OUTER) JOIN in our SQL-code

¹⁷ if SDSS or BOSS fibres were used

¹⁸ In g-r colour and z band absolute magnitudes.

A4 Millennium simulation data selection

For the galaxies in the selected snapshots of the WMAP7 re-run by Guo et al. (2013), we obtained the following parameters:

- galaxy ID (*galaxyID*)
- ID of their host FoF group (*fofID*)
- Cartesian coordinates (*x*, *y*, and *z*)
- proper motions (*velX*, *velY*, and *velZ*)
- absolute magnitudes in the griz bands *XDust*.

APPENDIX B: CATALOGUE DESCRIPTIONS

Alongside this paper¹⁹, we supply a set of catalogues containing the results of our group finder and our fundamental plane distance estimates. In Table B1, we provide our group catalogue that covers the SDSS spectroscopic footprint out to a redshift of 0.5. The individual galaxies associated with the groups listed in that table are provided in Table B2. The fundamental plane distances obtained using the traditional fundamental plane are listed in Table B3, while the distances from the corrected fundamental plane can be found in Table B4 and the distances obtained using the expanded fundamental plane are provided in Table B5.

¹⁹ The full catalogues will be made available on Vizier once this paper is accepted.

groupID	ra	dec	z	L_{obs}	σ_{group}	R_{group}	D_L	n_{group}
-	[$^{\circ}$]	[$^{\circ}$]	-	[$10^9 L_{\odot}$]	[km/s]	[$^{\circ}$]	[Mpc]	-
1	160.719162	59.227428	0.004273	270.5	708	10.018953	18.4	84
2	187.260452	10.417997	0.005818	4097.3	1201	4.531367	25.0	490
3	26.977180	27.432779	0.000520	0.2	0.0	0.0	2.2	1
4	189.997421	61.609196	0.000862	0.8	0.0	0.0	3.7	1
5	202.402115	58.418732	0.001072	0.3	0.0	0.0	4.6	1

Table B1. The first 5 lines of our combined SDSS/2MRS group catalogue to illustrate its data structure. First column: internal group ID of this catalogue; second and third column: equatorial coordinates of the group centre; fourth column: median redshift of the group; fifth column: combined i band luminosity of all detected members of the group; sixth column: velocity dispersion of the group; seventh column: angular radius of the group; eighth column: luminosity distance to the group centre; and ninth column: number of detected group members.

objID	groupID	ra	dec	z	rank
-	-	[$^{\circ}$]	[$^{\circ}$]	-	-
3	1	148.888260	69.065262	0.000161	32
40	2	186.549225	12.945970	0.000281	357
68	2	189.207565	13.162870	0.000290	395
239	1	146.814407	67.916382	0.000298	63
191	1	150.829758	68.733727	0.000332	46

Table B2. The first 5 lines of the associated galaxies list to group catalogue. First column: Object ID of the galaxy, which is either the SDSS Object ID or the line number in the 2MRS catalogue; second column: internal group ID to match with Table B1; third and fourth column: equatorial coordinates of the galaxy; fifth column: galaxy redshift in CMB rest frame; and sixth column: i band luminosity rank of the galaxy in its group.

objID	groupID	galID	ra	dec	z	$D_{L,ind}$	$D_{C,ind}$	$D_{A,ind}$	$D_{err,ind}$	z_{group}	$D_{L,group}$	$D_{C,group}$	$D_{A,group}$	$D_{err,group}$	n_{ETG}
-	-	-	[°]	[°]	-	[Mpc]	[Mpc]	[Mpc]	[%]	[Mpc]	[Mpc]	[Mpc]	[Mpc]	-	-
1237666184574271705	394809	572388	0.000563	34.985603	0.145205	647.2	569.1	500.4	20.2	0.145205	647.2	569.1	500.4	20.2	1
1237652900211261501	274279	418176	0.001718	-10.373803	0.203001	925.6	777.8	653.6	20.2	0.203001	925.6	777.8	653.6	20.2	1
1237663234987459169	552218	779260	0.002316	32.703094	0.171572	600.1	532.0	471.7	20.2	0.171572	600.1	532.0	471.7	20.2	1
1237678617417810259	608217	850134	0.003771	1.281564	0.249549	1091.7	894.7	733.2	20.2	0.249549	1091.7	894.7	733.2	20.2	1
1237652946378162349	581852	818225	0.004289	-10.946661	0.166433	878.9	744.0	629.8	20.2	0.166433	878.9	744.0	629.8	20.4	1
1237657191978959103	158813	264525	0.007252	0.731457	0.080279	433.7	396.3	362.0	20.2	0.080202	423.3	387.5	354.7	5.4	14

Table B3. The first five lines and another selected galaxy of our catalogue of uncorrected traditional fundamental plane distances. First column: SDSS object ID; second column: internal galaxy ID; third column: internal group ID; fourth and fifth column: equatorial coordinates of the galaxy; sixth column: galaxy redshift in CMB rest frame; seventh to ninth column: luminosity distance, co-moving distance, and angular diameter distance, respectively, of this galaxy derived from the fundamental plane; tenth column: relative error of the fundamental plane distance estimate; eleventh column: redshift of the galaxy group hosting the galaxy; twelfth to fourteenth column: luminosity distance, co-moving distance, and angular diameter distance, respectively, of the group hosting this galaxy derived from the fundamental plane; fifteenth column: relative error of the fundamental plane distance estimate to the group hosting this galaxy; and sixteenth column: total number of early-type galaxies in the same group as that galaxy.

objID	groupID	galID	ra	dec	z	$D_{L,ind}$	$D_{C,ind}$	$D_{A,ind}$	$D_{err,ind}$	z_{group}	$D_{L,group}$	$D_{C,group}$	$D_{A,group}$	$D_{err,group}$	n_{ETG}
-	-	-	[°]	[°]	-	[Mpc]	[Mpc]	[Mpc]	[%]	[Mpc]	[Mpc]	[Mpc]	[Mpc]	-	-
1237666184574271705	394809	572388	0.000563	34.985603	0.145205	676.8	592.2	518.1	15.9	0.145205	676.8	592.2	518.1	15.9	1
1237652900211261501	274279	418176	0.001718	-10.373803	0.203001	1066.9	877.6	721.8	15.9	0.203001	1066.9	877.6	721.8	15.2	1
1237663234987459169	552218	779260	0.002316	32.703094	0.171572	660.3	579.3	508.3	15.9	0.171572	660.3	579.3	508.3	15.9	1
1237678617417810259	608217	850134	0.003771	1.281564	0.249549	1190.5	961.8	777.1	15.9	0.249549	1190.5	961.8	777.1	15.9	1
1237652946378162349	581852	818225	0.004289	-10.946661	0.166433	882.6	746.7	631.7	15.9	0.166433	882.6	746.7	631.7	15.9	1
1237657191978959103	158813	264525	0.007252	0.731457	0.080279	292.1	274.3	257.6	15.9	0.080202	406.3	373.1	342.6	4.2	14

Table B4. The first five lines and another selected galaxy of our catalogue of corrected fundamental plane distances. Columns are the same as for Table B3.

objID	groupID	galID	ra	dec	z	$D_{L,ind}$	$D_{C,ind}$	$D_{A,ind}$	$D_{err,ind}$	z_{group}	$D_{L,group}$	$D_{C,group}$	$D_{A,group}$	$D_{err,group}$	n_{ETG}
-	-	-	[°]	[°]	-	[Mpc]	[Mpc]	[Mpc]	[%]	[Mpc]	[Mpc]	[Mpc]	[Mpc]	-	-
1237666184574271705	394809	572388	0.000563	34.985603	0.145205	737.8	638.9	553.3	9.6	0.145205	737.8	638.9	553.3	9.6	1
1237652900211261501	274279	418176	0.001718	-10.373803	0.203001	938.1	786.8	659.9	9.6	0.203001	938.1	786.8	659.9	9.6	1
1237663234987459169	552218	779260	0.002316	32.703094	0.171572	840.5	715.8	609.6	9.6	0.171572	840.5	715.8	609.6	9.6	1
1237678617417810259	608217	850134	0.003771	1.281564	0.249549	1351.2	1067.5	843.4	9.6	0.249549	1351.2	1067.5	843.4	9.6	1
1237652946378162349	581852	818225	0.004289	-10.946661	0.166433	837.1	713.3	607.9	9.6	0.166433	837.1	713.3	607.9	9.6	1
1237657191978959103	158813	264525	0.007252	0.731457	0.080279	407.1	373.8	343.2	9.6	0.080202	382.5	352.9	325.5	2.6	14

Table B5. The first five lines and another selected galaxy of our catalogue of expanded fundamental plane distances. Columns are the same as for Table B3.

APPENDIX C: ALTERNATIVE FUNDAMENTAL PLANE CALIBRATIONS

While investigating various ways to improve the traditional fundamental plane, we were testing several different alternative calibrations. While some ideas showed interesting correlations, none of them could reasonably compete with the other methods present in Sections 3.4, 3.5, and 3.6.

We tested using the number of early-type galaxies instead of the stellar masses for the expanded fundamental plane. While this apparently removed the systematic bias following the group richness, it did not fully account for the systematic offset at the lower redshifts (see Figure 19). The overall improvement compared to the traditional fundamental plane were marginal.

Instead of applying a correction in magnitude-redshift space after fitting the traditional fundamental plane, we considered letting the fundamental plane coefficients directly dependent on these parameters. We called this approach, in which we adapted the coefficient for the range of redshifts and magnitudes of our sample, the dynamical fundamental plane. We divided our sample into 2-dimensional bins in redshifts and apparent magnitude space and calculated the fundamental plane coefficients within individual in each bin. We then interpolated the between the values of the bins and used the coefficients corresponding to the observed redshift and magnitude of each galaxy. We found this distances obtained from this approach very sensitive to size of the bins and binning technique. Although the statistical error could be seemingly reduced to a few percent, the systematic redshift-dependences introduced this way were catastrophic.

We also tested the stellar mass fundamental plane and a slightly altered variant of it, which we called the modified stellar mass fundamental plane, with surprising results. As illustrated in Figure 11, the stellar mass roughly correlates with the absolute magnitudes as well as with the residuals of the fundamental plane. While we used the masses of Wisconsin method in this paper, we also tested this with the stellar masses of Maraston et al. (2009, 2013) obtained from SDSS photometry. While we consider the expanded fundamental plane as a safer approach to improve on fundamental plane distance, we also present a more challenging and experimental method, we found serendipitously by making a mistake when implementing the stellar mass fundamental plane. After some further testing and optimization, we ended up with the following definition:

$$\log_{10}(R_e) = a_{msm} \cdot \log_{10}(\sigma_0) + b_{msm}\Xi + c_{msm}. \quad (C1)$$

with

$$\Xi = \log_{10}(M_*) - f_{opt} \cdot \log_{10}(R_e) \quad (C2)$$

Again the index *msm* for the coefficients of the modified stellar mass fundamental plane should help to distinguish them from the coefficients of the traditional fundamental plane. We replaced the surface brightness term by a new variable Ξ that in the case of $f_{opt} = 2$ would turn Equation C1 into the stellar mass fundamental plane. The interesting thing about this calibration is that we included the physical radii of the galaxies as derived from redshift-based distances. This actually causes some circular reasoning, since we want to derive this parameter as independently from redshift as possible in order to use this relation as a proper standard rod for distance measurements. However, this is not only parameter entering the calibration, our approach seems to work just fine. While we found an uncertainty in the distance estimates derived from the (regular $f_{opt} = 2$) stellar mass fundamental plane of 23.6%,

with systematics due to redshift-space distortions of 1.5 percentage point, we were able to further reduce the scatter, when selecting other values for f_{opt} . We found that for a value of ~ 6.5 for f_{opt} , we were able to maximize a peculiar effect that we already found for $f_{opt} = 5$ ²⁰. When comparing the distances obtained from the modified stellar mass fundamental plane with the Tully-Fisher relation distances and the CosmicFlows-3 distances, we noticed that they agreed better with them than they did with redshift-based distances. The scatter between the modified fundamental plane distances and the Tully-Fisher relation/CosmicFlows-3 distances is smaller than the scatter between the modified fundamental plane distances and the redshift-based distances by about half a percentage point. This is a marginal but interesting feature. However, the systematics from the redshift-space distortions are huge, especially for the nearby galaxies (below a redshift of 0.03), where they are almost as big as the uncertainty of the modified stellar mass fundamental plane. Additionally, this was only the case for the photometric stellar masses of Maraston et al. (2009, 2013), but not for the spectro-photometric stellar masses obtained by the Wisconsin method (Chen et al. 2012) using Maraston models (Maraston & Strömbäck 2011).

APPENDIX D: COLOUR TRANSFORMATIONS BETWEEN SDSS AND 2MASS

In order to calculate magnitudes in SDSS bands from observed 2MASS (Skrutskie et al. 2006) magnitudes for our data from 2MRS (Huchra et al. 2012) or to calculate 2MASS magnitudes from the simulated SDSS magnitudes provides by the WMAP7 re-run of the Millennium simulation Guo et al. (2011), we had to use an extrapolation function. Following previous work of Bilir et al. (2008) and Saulder et al. (2016), we used the following equations for a extrapolations:

$$(m_g - m_{X_{2MASS}}) = d_{X_{2MASS}}(m_g - m_r) + e_{X_{2MASS}}(m_r - m_i) + f_{X_{2MASS}}, \quad (D1)$$

$$(m_r - m_{X_{2MASS}}) = d_{X_{2MASS}}(m_r - m_i) + e_{X_{2MASS}}(m_i - m_z) + f_{X_{2MASS}}, \quad (D2)$$

$$(m_{X_{SDSS}} - m_{K_s}) = d_{X_{SDSS}}(m_H - m_{K_s}) + e_{X_{SDSS}}(m_J - m_H) + f_{X_{SDSS}} \quad (D3)$$

The wild cards X_{2MASS} and X_{SDSS} stand for any of the 2MASS (J, H, and K_s) or SDSS (g, r, i, and z) respectively. Since we have four reliable²¹ SDSS bands, we had two options to set up the extrapolation function (using the magnitudes between the g and i band and alternatively using the magnitudes between the r and z band). m_g and similar terms express the magnitude (since we only deal with colours in all cases it does not matter if one uses apparent or absolute magnitudes as long as they consistent for each magnitude pair) in the corresponding filter. The coefficients d , e , and f for each possible function were determined by fitting the colour of the 5 890 galaxies that were identified in both SDSS and 2MRS. We filtered

²⁰ Due to a minor mistake in our initial derivation of the stellar mass fundamental plane, we had the value set to 5 by accident.

²¹ We excluded the u band for its well-known issues.

filter	equation	d	e	f	rms [mag]
J	D1	1.48 ± 0.03	1.09 ± 0.05	1.10 ± 0.02	0.178
H	D1	1.53 ± 0.03	1.31 ± 0.05	1.67 ± 0.02	0.194
K	D1	1.43 ± 0.03	1.48 ± 0.06	1.93 ± 0.02	0.216
J	D2	1.44 ± 0.04	0.26 ± 0.02	1.25 ± 0.02	0.181
H	D2	1.68 ± 0.04	0.37 ± 0.03	1.82 ± 0.02	0.196
K	D2	1.73 ± 0.05	0.48 ± 0.03	2.02 ± 0.02	0.214
g	D3	1.06 ± 0.03	1.21 ± 0.04	2.42 ± 0.03	0.253
r	D3	1.06 ± 0.02	1.07 ± 0.03	1.79 ± 0.02	0.201
i	D3	1.02 ± 0.02	0.96 ± 0.03	1.50 ± 0.02	0.185
z	D3	0.90 ± 0.02	0.76 ± 0.03	1.51 ± 0.02	0.194

Table D1. Coefficients for all derived colour transformations.

iteratively for $5 - \sigma$ outliers, which marginally reduced our sample to 5 842 galaxies.

We list the coefficients for all filters using all equations in Table D1. We are able to estimate the colour (and thereby magnitude) of a galaxy in a different filter system with an uncertainty of about 0.2 mag. This naturally varies depending on the distance between the central wave length of the corresponding filters used²².

This paper has been typeset from a $\text{\TeX}/\text{\LaTeX}$ file prepared by the author.

²² Oddly enough, both equations used for SDSS filters perform about the same, but in two cases the actually closer filter system (riz) yields marginally worth results than other set of filters.